Aqueous-phase mechanism for secondary organic aerosol formation from isoprene: application to the Southeast United States and co-benefit of SO_2 emission controls

E. A. Marais[1], D. J. Jacob[1,2], J. L. Jimenez[3,4], P. Campuzano-Jost[3,4], D. A. Day[3,4], W. Hu[3,4], J. Krechmer[3,4], L. Zhu[1], P. S. Kim[2], C. C. Miller[2], J. A. Fisher[5], K. Travis[1], K. Yu[1], T. F. Hanisco[6], G. M. Wolfe[6,7], H. L. Arkinson[8], H. O. T. Pye[9], K. D. Froyd[3,10], J. Liao[3,10], V. F. McNeill[11]

[1]School of Engineering and Applied Sciences, Harvard University, Cambridge, MA, USA.
[2]Earth and Planetary Sciences, Harvard University, Cambridge, MA, USA.
[3]Cooperative Institute for Research in Environmental Sciences, University of Colorado, Boulder, CO, USA.
[4]Department of Chemistry and Biochemistry, University of Colorado, Boulder, CO, USA.
[5]School of Chemistry and School of Earth and Environmental Sciences, University of Wollongong, Wollongong, New South Wales, Australia.
[6]Atmospheric Chemistry and Dynamics Lab, NASA Goddard Space Flight Center, Greenbelt, MD, USA.
[7]Joint Center for Earth Systems Technology, University of Maryland Baltimore County, Baltimore, MD, USA.
[8]Department of Atmospheric and Oceanic Science, University of Maryland, College Park, MD, USA.
[9]National Exposure Research Laboratory, US EPA, Research Triangle Park, NC, USA.
[10]Chemical Sciences Division, Earth System Research Laboratory, NOAA, Boulder, Colorado, USA
[11]Department of Chemical Engineering, Columbia University, New York, New York 10027, USA.

Abstract

Isoprene emitted by vegetation is an important precursor of secondary organic aerosol (SOA), but the mechanism and yields are uncertain. Aerosol is prevailingly aqueous under the humid conditions typical of isoprene-emitting regions. Here we develop an aqueous-phase mechanism for isoprene SOA formation coupled to a detailed gas-phase isoprene oxidation scheme. The mechanism is based on aerosol reactive uptake coefficients (γ) for water-soluble isoprene oxidation products, including sensitivity to aerosol acidity and nucleophile concentrations. We apply this mechanism to simulation of aircraft (SEAC^{4}RS) and ground-based (SOAS) observations over the Southeast US in summer 2013 using the GEOS-Chem chemical transport model. Emissions of nitrogen oxides ($NO_x \equiv NO + NO_2$) over the Southeast US are such that the peroxy radicals produced from isoprene oxidation ($ISOPO_2$) react significantly with both NO (high-NO_x pathway) and HO_2 (low-NO_x pathway), leading to different suites of isoprene SOA precursors. We find a mean SOA mass yield of 3.3 % from isoprene oxidation, consistent with the observed relationship of total fine organic aerosol (OA) and formaldehyde (a product of isoprene oxidation). Isoprene SOA production is mainly contributed by two immediate gas-phase precursors, isoprene epoxydiols (IEPOX, 58% of isoprene SOA) from the low-NO_x pathway and glyoxal (28%) from both low- and high-NO_x pathways. This speciation is consistent with observations of IEPOX SOA from SOAS and SEAC^{4}RS. Observations show a strong relationship between IEPOX SOA and sulfate aerosol that we explain as due to the effect of sulfate on aerosol acidity and volume. Isoprene SOA concentrations increase as NO_x emissions decrease (favoring the low-NO_x pathway for isoprene oxidation), but decrease more

strongly as SO_2 emissions decrease (due to the effect of sulfate on aerosol acidity and volume). The US EPA projects 2013-2025 decreases in anthropogenic emissions of 34% for NO_x (leading to 7% increase in isoprene SOA) and 48% for SO_2 (35% decrease in isoprene SOA). Reducing SO_2 emissions decreases sulfate and isoprene SOA by a similar magnitude, representing a factor of 2 co-benefit for $PM_{2.5}$ from SO_2 emission controls.

Keywords: isoprene, SOA yield, IEPOX, glyoxal, SEAC^{4}RS, SOAS, formaldehyde.

Corresponding Author: emarais@seas.harvard.edu

1. Introduction

Isoprene emitted by vegetation is a major source of secondary organic aerosol (SOA) (Carlton et al., 2009, and references therein) with effects on human health, visibility, and climate. There is large uncertainty in the yield and composition of isoprene SOA (Scott et al., 2014; McNeill et al., 2014), involving a cascade of species produced in the gas-phase oxidation of isoprene and their interaction with pre-existing aerosol (Hallquist et al., 2009). We develop here a new aqueous-phase mechanism for isoprene SOA formation coupled to gas-phase chemistry, implement it in the GEOS-Chem chemical transport model (CTM) to simulate observations in the Southeast US, and from there derive new constraints on isoprene SOA yields and the contributing pathways.

Organic aerosol is ubiquitous in the atmosphere, often dominating fine aerosol mass (Zhang et al., 2007), including in the Southeast US where it accounts for more than 60% in summer (Attwood et al., 2014). It may be directly emitted by combustion as primary organic aerosol (POA), or produced within the atmosphere as SOA by oxidation of volatile organic compounds (VOCs). Isoprene (C_5H_8) from vegetation is the dominant VOC emitted globally, and the Southeast US in summer is one of the largest isoprene-emitting regions in the world (Guenther et al., 2006). SOA yields from isoprene are low compared with larger VOCs (Pye et al., 2010), but isoprene emissions are much higher. Kim et al. (2015) estimated that isoprene accounts for 40% of total organic aerosol in the Southeast US in summer.

Formation of OA from oxidation of isoprene depends on local concentrations of nitrogen oxide radicals ($NO_x \equiv NO + NO_2$) and pre-existing aerosol. NO_x concentrations determine the fate of organic peroxy radicals originating from isoprene oxidation ($ISOPO_2$), leading to different cascades of oxidation products in the low-NO_x and high-NO_x pathways (Paulot et al.,

2009a; 2009b). Uptake of isoprene oxidation products to the aerosol phase depends on their vapor pressure (Donahue et al., 2006), solubility in aqueous media (Saxena and Hildeman, 1996), and subsequent condensed-phase reactions (Volkamer et al., 2007). Aqueous aerosol provides a medium for reactive uptake (Eddingsaas et al., 2010; Surratt et al., 2010) with dependences on acidity (Surratt et al., 2007a), concentration of nucleophiles such as sulfate (Surratt et al., 2007b), aerosol water (Carlton and Turpin, 2013), and organic coatings (Gaston et al., 2014).

We compile in Fig. 1 the published laboratory yields of isoprene SOA as a function of initial NO concentration and relative humidity (RH). Here and elsewhere, the isoprene SOA yield is defined as the mass of SOA produced per unit mass of isoprene oxidized. Isoprene SOA yields span a wide range, from <0.1% to >10%, with no systematic difference between low-NO_x and high-NO_x pathways. Yields tend to be higher in dry chambers (RH < 10%). Under such dry conditions isoprene SOA is expected to be solid (Virtanen et al., 2010; Song et al., 2015). At humid conditions more representative of the summertime boundary layer, aerosols are likely aqueous (Bateman et al., 2014). Standard isoprene SOA mechanisms used in atmospheric models assume reversible partitioning onto pre-existing organic aerosol, fitting the dry chamber data (Odum et al., 1996). However, this may not be appropriate for actual atmospheric conditions where aqueous-phase chemistry with irreversible reactive uptake of water-soluble gases is likely the dominant mechanism (Ervens et al., 2011; Carlton and Turpin, 2013). Several regional/global models have implemented mechanisms for aqueous-phase formation of isoprene SOA (Fu et al., 2008, 2009; Carlton et al., 2008; Myriokefalitakis et al., 2011; Liu et al., 2012; Pye et al., 2013; Lin et al., 2014).

Here we present a mechanism for irreversible aqueous-phase isoprene SOA formation integrated within a detailed chemical mechanism for isoprene gas-phase oxidation, thus linking isoprene SOA formation to gas-phase chemistry and avoiding more generic volatility-based parameterizations that assume dry organic aerosol (Odum et al., 1996; Donahue et al., 2006). We use this mechanism in the GEOS-Chem CTM to simulate observations from the SOAS (surface) and SEAC^{4}RS (aircraft) field campaigns over the Southeast US in summer 2013, with focus on isoprene SOA components and on the relationship between OA and formaldehyde (HCHO). HCHO is a high-yield oxidation product of isoprene (Palmer et al., 2003) and we use the OA-HCHO relationship as a constraint on isoprene SOA yields. SOAS measurements were made at a ground site in rural Centreville, Alabama (Hu et al., 2015; http://soas2013.rutgers.edu/). SEAC^{4}RS measurements were made from the NASA DC-8 aircraft with extensive boundary layer coverage across the Southeast (Toon et al., 2016; SEAC^{4}RS Archive).

2. Chemical mechanism for isoprene SOA formation

The default treatment of isoprene SOA in GEOS-Chem at the time of this work (v9-02; http://geos-chem.org) followed a standard parameterization operating independently from the gas-phase chemistry mechanism and based on reversible partitioning onto pre-existing OA of generic semivolatile products of isoprene oxidation by OH and NO_3 radicals (Pye et al., 2010). Here we implement a new mechanism for reactive uptake by aqueous aerosols of species produced in the isoprene oxidation cascade of the GEOS-Chem gas-phase mechanism. This couples SOA formation to the gas-phase chemistry and is in accord with increased evidence for a major role of aqueous aerosols in isoprene SOA formation (Ervens et al., 2011).

The standard gas-phase isoprene oxidation mechanism in GEOS-Chem v9-02 is described in Mao et al. (2013) and is based on best knowledge at the time building on mechanisms for the oxidation of isoprene by OH (Paulot et al., 2009a; 2009b) and NO_3 (Rollins et al., 2009). Updates implemented in this work are described below and in companion papers applying GEOS-Chem to simulation of observed gas-phase isoprene oxidation products over the Southeast US in summer 2013 (Fisher et al., 2016; Travis et al., 2016). Most gas-phase products of the isoprene oxidation cascade in GEOS-Chem have high dry deposition velocity, competing in some cases with removal by oxidation and aerosol formation (Nguyen et al., 2015a; Travis et al., 2016).

Figure 2 shows the isoprene oxidation cascade in GEOS-Chem leading to SOA formation. Reaction pathways leading to isoprene SOA precursors are described below. Yields are in mass percent, unless stated otherwise. Reactive $ISOPO_2$ isomers formed in the first OH oxidation step react with NO, the hydroperoxyl radical (HO_2), other peroxy radicals (RO_2), or undergo isomerization (Peeters et al., 2009). The NO reaction pathway (high-NO_x pathway) yields C_5 hydroxy carbonyls, methyl vinyl ketone, methacrolein, and first-generation isoprene nitrates (ISOPN). The first three products go on to produce glyoxal and methylglyoxal, which serve as SOA precursors. The overall yield of glyoxal from the high-NO_x pathway is 7 mol % (yield on a molar basis). Oxidation of ISOPN by OH and O_3 is as described by Lee et al. (2014). Reaction of ISOPN with OH produces saturated dihydroxy dinitrates (DHDN), 21 and 27 mol % from the beta and delta channels respectively (Lee et al., 2014), and 10 mol % isoprene epoxydiols (IEPOX) from each channel (Jacobs et al., 2014). We also adopt the mechanism of Lin et al. (2013) to generate C_4 hydroxyepoxides (methacrylic acid epoxide and hydroxymethylmethyl-α-lactone, both denoted MEPOX) from OH oxidation of a

141 peroxyacylnitrate formed when methacrolein reacts with OH followed by NO_2. Only
142 hydroxymethylmethyl-α-lactone is shown in Fig. 2.
143 The HO_2 reaction pathway for $ISOPO_2$ leads to formation of hydroxyhydroperoxides
144 (ISOPOOH) that are oxidized to IEPOX (Paulot et al., 2009b) and several low-volatility
145 products, represented here as C_5-LVOC (Krechmer et al., 2015). The kinetics of IEPOX
146 oxidation by OH is uncertain, and experimentally determined IEPOX lifetimes vary from 8 to 28
147 h for an OH concentration of 1×10^6 molecules cm^{-3} (Jacobs et al., 2013; Bates et al., 2014). In
148 GEOS-Chem we apply the fast kinetics of Jacobs et al. (2013) and reduce the yield of IEPOX
149 from ISOPOOH from 100 to 75%, within the range observed by St. Clair et al. (2016), to address
150 a factor of 4 overestimate in simulated IEPOX pointed out by Nguyen et al. (2015a). The IEPOX
151 discrepancy could alternatively be addressed with an order-of-magnitude increase in uptake by
152 aerosol (see below) but the model would then greatly overestimate the observed IEPOX SOA
153 concentrations in SOAS and SEAC^{4}RS (Section 4).
154 IEPOX oxidizes to form glyoxal and methylglyoxal (Bates et al., 2014). The overall
155 glyoxal yield from the $ISOPO_2 + HO_2$ pathway is 6 mol %. Krechmer et al. (2015) report a 2.5
156 mol % yield of C_5-LVOC from ISOPOOH but we reduce this to 0.5 mol % to reproduce surface
157 observations of the corresponding aerosol products (Section 4). Methyl vinyl ketone and
158 methacrolein yields from the $ISOPO_2 + HO_2$ pathway are 2.5 and 3.8 mol %, respectively (Liu et
159 al., 2013), sufficiently low that they do not lead to significant SOA formation.
160 Minor channels for $ISOPO_2$ are isomerization and reaction with RO_2. Isomerization
161 forms hydroperoxyaldehydes (HPALD) that go on to photolyze, but products are uncertain
162 (Peeters and Müller, 2010). We assume 25 mol % yield each of glyoxal and methylglyoxal from
163 HPALD photolysis in GEOS-Chem following Stavrakou et al. (2010). Reaction of $ISOPO_2$ with

164 RO_2 leads to the same suite of C_4-C_5 carbonyls as reaction with NO (C_5 hydroxy carbonyls,
165 methacrolein, and methyl vinyl ketone) and from there to glyoxal and methylglyoxal.
166 Immediate aerosol precursors from the isoprene + OH oxidation cascade are identified in
167 Fig. 2. For the high-NO_x pathway ($ISOPO_2$ + NO channel) these include glyoxal and
168 methylglyoxal (McNeill et al., 2012), ISOPN (Darer et al., 2011; Hu et al., 2011), DHDN (Lee et
169 al., 2014), MEPOX (Lin et al., 2013), and IEPOX (Jacobs et al., 2014). For the low-NO_x
170 pathway ($ISOPO_2$ + HO_2 channel) aerosol precursors are IEPOX (Eddingsaas et al., 2010), C_5-
171 LVOC (Krechmer et al., 2015, in which the aerosol-phase species is denoted ISOPOOH-SOA),
172 glyoxal, and methylglyoxal. Glyoxal and methylglyoxal are also produced from the $ISOPO_2$ +
173 RO_2 and $ISOPO_2$ isomerization channels.
174 Ozonolysis and oxidation by NO_3 are additional minor isoprene reaction pathways (Fig.
175 2). The NO_3 oxidation pathway is a potentially important source of isoprene SOA at night
176 (Brown et al., 2009) from the irreversible uptake of low-volatility second-generation
177 hydroxynitrates (NT-ISOPN) (Ng et al., 2008; Rollins et al., 2009). We update the gas-phase
178 chemistry of Rollins et al. (2009) as implemented by Mao et al. (2013) to include formation of 4
179 mol % of the aerosol-phase precursor NT-ISOPN from first-generation alkylnitrates (Rollins et
180 al., 2009). Ozonolysis products are volatile and observed SOA yields in chamber studies are low
181 (< 1%; Kleindienst et al., 2007). In GEOS-Chem only methylglyoxal is an aerosol precursor
182 from isoprene ozonolysis.
183 We implement uptake of isoprene oxidation products to aqueous aerosols using
184 laboratory-derived reactive uptake coefficients (γ) as given by Anttila et al. (2006) and Gaston et
185 al. (2014):
186

$$\gamma = \left[\frac{1}{\alpha} + \frac{3\omega}{4rRTH^{*}k_{aq}} \right]^{-1} \quad (1).$$

Here α is the mass accommodation coefficient (taken as 0.1 for all immediate SOA precursors in Fig. 2), ω is the mean gas-phase molecular speed (cm s^{-1}), r is the aqueous particle radius (cm), R is the universal gas constant (0.08206 L atm K^{-1} mol^{-1}), T is temperature (K), H^{*} is the effective Henry's Law constant (M atm^{-1}) accounting for any fast dissociation equilibria in the aqueous phase, and k_{aq} is the pseudo first-order aqueous-phase reaction rate constant (s^{-1}) for conversion to non-volatile products.

Precursors with epoxide functionality, IEPOX and MEPOX, undergo acid-catalyzed epoxide ring opening and nucleophilic addition in the aqueous phase. The aqueous-phase rate constant formulation is from Eddingsaas et al. (2010),

$$k_{aq} = k_{\mathrm{H^+}}\left[\mathrm{H^+}\right] + k_{nuc}\left[nuc\right]\left[\mathrm{H^+}\right] + k_{HSO_4^-}\left[\mathrm{HSO_4^-}\right] \quad (2),$$

and includes three channels: acid-catalyzed ring opening followed by nucleophilic addition of H_2O ($k_{\mathrm{H^+}}$ in M^{-1} s^{-1}) leading to methyltetrols, acid-catalyzed ring opening followed by nucleophilic addition of sulfate and nitrate ions ($nuc \equiv SO_4^{2-} + NO_3^-$, k_{nuc} in M^{-2} s^{-1}) leading to organosulfates and organonitrates, and concerted protonation and nucleophilic addition by bisulfate, HSO_4^- (k_{HSO4-} in M^{-1} s^{-1}), leading to organosulfates.

Precursors with nitrate functionality ($-ONO_2$), ISOPN and DHDN, hydrolyze to form low-volatility polyols and nitric acid (Hu et al., 2011; Jacobs et al., 2014), so k_{aq} in Eq. (1) is the hydrolysis rate constant.

Glyoxal and methylglyoxal form SOA irreversibly by surface uptake followed by aqueous-phase oxidation and oligomerization to yield non-volatile products (Liggio et al., 2005; Volkamer et al., 2009; Nozière et al., 2009; Ervens et al., 2011; Knote et al., 2014). Glyoxal forms SOA with higher yields during the day than at night due to OH aqueous-phase chemistry (Tan et al., 2009; Volkamer et al., 2009; Summer et al., 2014). We use a daytime γ of 2.9×10^{-3} for glyoxal from Liggio et al. (2005) and a nighttime γ of 5×10^{-6} (Waxman et al., 2013; Sumner et al., 2014). The SOA yield of methylglyoxal is small compared with that of glyoxal (McNeill et al., 2012). A previous GEOS-Chem study by Fu et al. (2008) used the same γ (2.9×10^{-3}) for glyoxal and methylglyoxal. Reaction rate constants are similar for aqueous-phase processing of glyoxal and methylglyoxal (Buxton et al., 1997; Ervens et al., 2003), but H^* of glyoxal is about 4 orders of magnitude higher. Here we scale the γ for methylglyoxal to the ratio of effective Henry's law constants: $H^* = 3.7 \times 10^3$ M atm^{-1} for methylglyoxal (Tan et al., 2010) and $H^* = 2.7 \times 10^7$ M atm^{-1} for glyoxal (Sumner et al., 2014). The resulting uptake of methylglyoxal is very slow and makes a negligible contribution to isoprene SOA.

The species C_5-LVOC from ISOPOOH oxidation and NT-ISOPN from isoprene reaction with NO_3 have very low volatility and are assumed to condense to aerosols with a γ of 0.1 limited by mass accommodation. Results are insensitive to the precise value of γ since uptake by aerosols is the main sink for these species in any case.

Table 1 gives input variables used to calculate γ for IEPOX, ISOPN, and DHDN by Eqs. (1) and (2). Rate constants are from experiments in concentrated media, representative of aqueous aerosols, so no activity correction factors are applied. Reported experimental values of k_{H+} vary by an order of magnitude from 1.2×10^{-3} M^{-1} s^{-1} (Eddingsaas et al., 2010) to 3.6×10^{-2} M^{-1} s^{-1} (Cole-Filipiak et al., 2010). Values of k_{nuc} vary by 3 orders of magnitude from 2×10^{-4} M^{-}

^{2} s^{-1} (Eddingsaas et al., 2010) to 5.2×10^{-1} M^{-2} s^{-1} (Piletic et al., 2013). Reported values of IEPOX H^* vary by two orders of magnitude (Eddingsaas et al., 2010; Nguyen et al., 2014). We chose values of k_{H+}, k_{nuc}, and H^* to fit the SOAS and SEAC^{4}RS observations of total IEPOX SOA and IEPOX organosulfates, as discussed in Section 4.

Table 2 lists average values of γ for all immediate aerosol precursors in the Southeast US boundary layer in summer as simulated by GEOS-Chem (Section 3). γ for IEPOX is a strong function of pH and increases from 1×10^{-4} to 1×10^{-2} as pH decreases from 3 to 0. Gaston et al. (2014) reported order-of-magnitude higher values of γ for IEPOX, reflecting their use of a higher H^*, but this would lead in our model to an overestimate of IEPOX SOA observations (Section 4). The value of γ for MEPOX is assumed to be 30 times lower than that of IEPOX when the aerosol is acidic (pH < 4), due to slower acid-catalyzed ring opening (Piletic et al., 2013; Riedel et al., 2015). At pH > 4 we assume that γ for IEPOX and MEPOX are the same (Riedel et al., 2015), but they are then very low.

Isoprene SOA formation in clouds is not considered here. Acid-catalyzed pathways would be slow. Observations show that the isoprene SOA yield in the presence of laboratory-generated clouds is low (0.2-0.4%; Brégonzio-Rozier et al., 2015). Wagner et al. (2015) found no significant production of SOA in boundary layer clouds over the Southeast US during SEAC^{4}RS.

3. GEOS-Chem simulation and isoprene SOA yields

Several companion papers apply GEOS-Chem to interpret SEAC^{4}RS and surface data over the Southeast US in summer 2013 including Kim et al. (2015) for aerosols, Fisher et al. (2016) for organic nitrates, Travis et al. (2016) for ozone and NO_x, and Zhu et al. (2016) for HCHO. These studies use a model version with 0.25° × 0.3125° horizontal resolution over North

America, nested within a 4° × 5° global simulation. Here we use a 2° × 2.5° global GEOS-Chem simulation with no nesting. Yu et al. (2016) found little difference between 0.25° × 0.3125° and 2° × 2.5° resolutions in simulated regional statistics for isoprene chemistry.

The reader is referred to Kim et al. (2015) for a general presentation of the model, the treatment of aerosol sources and sinks, and evaluation with Southeast US aerosol observations; and to Travis et al. (2016) and Fisher et al. (2016) for presentation of gas-phase chemistry and comparisons with observed gas-phase isoprene oxidation products. Isoprene emission is from the MEGAN v2.1 inventory (Guenther et al., 2012). The companion papers decrease isoprene emission by 15% from the MEGAN v2.1 values to fit the HCHO data (Zhu et al., 2016), but this is not applied here.

Our SOA simulation differs from that of Kim et al. (2015). They assumed fixed 3% and 10% mass yields of SOA from isoprene and monoterpenes, respectively, and parameterized SOA formation from anthropogenic and open fire sources as a kinetic irreversible process following Hodzic and Jimenez (2011). Here we use our new aqueous-phase mechanism for isoprene SOA coupled to gas-phase chemistry as described in Section 2, and otherwise use the semivolatile reversible partitioning scheme of Pye et al. (2010) for monoterpene, anthropogenic, and open fire SOA. Kim et al. (2015) found no systematic bias in detailed comparisons to OA measurements from SEAC^{4}RS and from surface networks. We find a low bias, as shown below, because the reversible partitioning scheme yields low anthropogenic and open fire SOA concentrations.

Organic aerosol and sulfate contribute most of the aerosol mass over the Southeast US in summer, while nitrate is negligibly small (Kim et al., 2015). GEOS-Chem uses the ISORROPIA thermodynamic model (Fountoukis and Nenes, 2007) to simulate sulfate-nitrate-ammonium (SNA) aerosol composition, water content, and acidity as a function of local conditions.

Simulated aerosol pH along the SEAC^{4}RS flight tracks in the Southeast US boundary layer averages 1.3 (interquartiles 0.92 and 1.8). The aerosol pH remains below 3 even when sulfate aerosol is fully neutralized by ammonia (Guo et al., 2015).

We consider that the aqueous aerosol population where isoprene SOA formation can take place is defined by the sulfate aerosol population. This assumes that all aqueous aerosol particles contain some sulfate, and that all sulfate is aqueous. Clear-sky RH measured from the aircraft in the Southeast US boundary layer during SEAC^{4}RS averaged 72 ± 17%, and the corresponding values in GEOS-Chem sampled along the flight tracks averaged 66 ± 16%). These RHs are sufficiently high that sulfate aerosol can reliably be expected to be aqueous (Wang et al., 2008). The rate of gas uptake by the sulfate aerosol is computed with the pseudo-first order reaction rate constant k_{het} (s^{-1}) (Schwartz, 1986; Jacob, 2000):

$$k_{het} = \int_0^\infty 4\pi r^2 \left(\frac{r}{D_g} + \frac{4}{\gamma\omega} \right)^{-1} n(r)dr \quad (3),$$

where D_g is the gas-phase diffusion constant (taken to be 0.1 $cm^2\ s^{-1}$) and $n(r)$ is the number size distribution of sulfate aerosol (cm^{-4}). The first and second terms in parentheses describe the limitations to gas uptake from gas-phase diffusion and aqueous-phase reaction, respectively.

The sulfate aerosol size distribution including RH-dependent hygroscopic growth factors is from the Global Aerosol Data Set (GADS) of Koepke et al. (1997), as originally implemented in GEOS-Chem by Martin et al. (2003) and updated by Drury et al. (2010). The GADS size distribution compares well with observations over the eastern US in summer (Drury et al., 2010), including for SEAC^{4}RS (Kim et al., 2015). We compute $n(r)$ locally in GEOS-Chem by taking

300 the dry SNA mass concentration, converting from mass to volume with a dry aerosol mass
301 density of 1700 kg m^{-3} (Hess et al., 1998), applying the aerosol volume to the dry sulfate size
302 distribution in GADS, and then applying the GADS hygroscopic growth factors. We verified that
303 the hygroscopic growth factors from GADS agree within 10% with those computed locally from
304 ISORROPIA.

305 Figure 2 shows the mean branching ratios for isoprene oxidation in the Southeast US
306 boundary layer as calculated by GEOS-Chem. 87% of isoprene reacts with OH, 8% with ozone,
307 and 5% with NO_3. Oxidation of isoprene by OH produces $ISOPO_2$ of which 51% reacts with NO
308 (high-NO_x pathway), 35% reacts with HO_2, 8% isomerizes, and 6% reacts with other RO_2
309 radicals.

310 Glyoxal is an aerosol precursor common to all isoprene + OH pathways in our
311 mechanism with yields of 7 mol % from the $ISOPO_2$ + NO pathway, 6 mol % from $ISOPO_2$ +
312 HO_2, 11 mol % from $ISOPO_2$ + RO_2, and 25 mol % from $ISOPO_2$ isomerization. For the
313 Southeast US conditions we thus find that 44% of glyoxal is from the $ISOPO_2$ + NO pathway,
314 24% from $ISOPO_2$ + HO_2, 8% from $ISOPO_2$ + RO_2, and 24% from $ISOPO_2$ isomerization.

315 The mean total yield of isoprene SOA computed in GEOS-Chem for the Southeast US
316 boundary layer is 3.3%, as shown in Fig. 2. IEPOX contributes 1.9% and glyoxal 0.9%. The low-
317 NO_x pathway involving $ISOPO_2$ reaction with HO_2 contributes 73% of the total isoprene SOA
318 yield, mostly from IEPOX, even though this pathway is only 35% of the fate of $ISOPO_2$. The
319 high-NO_x pathway contributes 16% of isoprene SOA, mostly from glyoxal. MEPOX
320 contribution to isoprene SOA is small (2%) and consistent with a recent laboratory study that
321 finds low SOA yields from this pathway under humid conditions (Nguyen et al., 2015b). The
322 minor low-NO_x pathways from $ISOPO_2$ isomerization and reaction with RO_2 contribute 8% of

isoprene SOA through glyoxal. The remainder of isoprene SOA formation (3%) is from nighttime oxidation by NO_3.

The dominance of IEPOX and glyoxal as precursors for isoprene SOA was previously found by McNeill et al. (2012) using a photochemical box model. Both IEPOX and glyoxal are produced photochemically, and both are removed photochemically in the gas phase by reaction with OH (and photolysis for glyoxal). The mean lifetimes of IEPOX and glyoxal against gas-phase photochemical loss average 1.6 and 2.3 h respectively for SEAC^{4}RS daytime conditions; mean lifetimes against reactive uptake by aerosol are 31 and 20 hours, respectively. For both species, aerosol uptake is thus a minor sink competing with gas-phase photochemical loss. Although we have assumed here the fast gas-phase kinetics from Jacobs et al. (2013) for the IEPOX + OH reaction, this result would not change if we used the slower kinetics from Bates et al. (2014).

The dominance of gas-phase loss over aerosol uptake for both IEPOX and glyoxal implies that isoprene SOA formation is highly sensitive to their reactive uptake coefficients γ and to the aqueous aerosol mass concentration (in both cases, γ is small enough that uptake is controlled by bulk aqueous-phase rather than surface reactions). We find under SEAC^{4}RS conditions that γ for IEPOX is mainly controlled by the H^+ concentration ($k_{H+}[H^+]$ in Eq. (2)), with little contribution from nucleophile-driven and HSO_4^--driven channels, although this is based on highly uncertain rate constants (Section 2). Consistency with SOAS and SEAC^{4}RS observations will be discussed below.

The 3.3% mean yield of isoprene SOA from our mechanism is consistent with the fixed yield of 3% assumed by Kim et al. (2015) in their GEOS-Chem simulation of the SEAC^{4}RS period, including extensive comparisons to OA observations that showed a 40% mean

346 contribution of isoprene to total OA. We conducted a sensitivity simulation using the default
347 isoprene SOA mechanism in GEOS-Chem based on reversible partitioning of semivolatile
348 oxidation products onto pre-existing OA (Pye et al., 2010). The isoprene SOA yield in that
349 simulation was only 1.1%. The observed correlation of OA with HCHO in SEAC^{4}RS supports
350 our higher yield, as shown below.
351
352 **4. Observational constraints on isoprene SOA yields**
353 Isoprene is the largest source of HCHO in the Southeast US (Millet et al., 2006), and we
354 use the observed relationship between OA and HCHO to evaluate the GEOS-Chem isoprene
355 SOA yields. The SEAC^{4}RS aircraft payload included measurements of OA from an Aerodyne
356 Aerosol Mass Spectrometer (HR-ToF-AMS; DeCarlo et al, 2006; Canagaratna et al, 2007)
357 concurrent with HCHO from a laser-induced fluorescence instrument (ISAF; Cazorla et al.,
358 2015). Column HCHO was also measured during SEAC^{4}RS from the OMI satellite instrument
359 (González Abad et al., 2015; Zhu et al., 2016), providing a proxy for isoprene emission (Palmer
360 et al., 2003; 2006).
361 Figure 3 (left) shows the observed and simulated relationships between OA and HCHO
362 mixing ratios in the boundary layer. There is a strong correlation in the observations and in the
363 model (R = 0.79 and R = 0.82, respectively). OA simulated with our aqueous-phase isoprene
364 SOA mechanism reproduces the observed slope (2.8 ± 0.3 μg sm^{-3} ppbv^{-1}, vs. 3.0 ± 0.4 μg sm^{-3}
365 ppbv^{-1} in the observations). Similarly strong correlations and consistency between model and
366 observations are found with column HCHO measured from OMI (Fig. 3, right). The estimated
367 error on individual OMI HCHO observations is about 30% (Millet et al., 2006).

Also shown in Fig. 3 is a sensitivity simulation with the default GEOS-Chem mechanism based on reversible partitioning with pre-existing organic aerosol (Pye et al., 2010) and producing a 1.1% mean isoprene SOA yield, as compared to 3.3% in our simulation with the aqueous-phase mechanism. That sensitivity simulation shows the same OA-HCHO correlation ($R = 0.82$) but underestimates the slope (2.0 ± 0.3 μg sm^{-3} $ppbv^{-1}$). The factor of 3 increase in our isoprene SOA yield does not induce a proportional increase in the slope, as isoprene contributes only ~ 40% of OA in the Southeast US. But the slope is sensitive to the isoprene SOA yield, and the good agreement between our simulation and observations supports our estimate of a mean 3.3% yield for the Southeast US.

Figure 3 shows an offset between the model and observations illustrated by the regression lines. We overestimate HCHO by 0.4 ppbv on average because we did not apply the 15% downward correction to MEGAN v2.1 isoprene emissions (Zhu et al., 2016). We also underestimate total OA measured by the AMS in the boundary layer by 1.1 μg sm^{-3} (mean AMS OA is 5.8 ± 4.3 μg sm^{-3}; model OA is 4.7 ± 4.4 μg sm^{-3}). The bias can be explained by our omission of anthropogenic and open fire SOA, found by Kim et al. (2015) to account on average for 18% of OA in SEAC^{4}RS.

Figure 4 shows time series of the isoprene SOA components IEPOX SOA and C_5-LVOC SOA at Centreville, Alabama during SOAS. AMS observations from Hu et al. (2015) and Krechmer et al. (2015) are compared to model values. IEPOX SOA and C_5-LVOC SOA are on average 17% and 2% of total AMS OA, respectively (Hu et al., 2015; Krechmer et al., 2015). The model reproduces mean IEPOX SOA and C_5-LVOC SOA without bias, supporting the conclusion that IEPOX is the dominant contributor to isoprene SOA in the Southeast US (Fig. 2).

Figure 5 shows the relationships of daily mean IEPOX SOA and sulfate concentrations at Centreville and in the SEAC^{4}RS boundary layer. The same factor analysis method was used to derive IEPOX SOA in SEAC^{4}RS as in SOAS, however the uncertainty is larger for the aircraft observations due to the much wider range of conditions encountered. There is a strong correlation between IEPOX SOA and sulfate, both in observations and the model, with similar slopes. Correlation between IEPOX SOA and sulfate has similarly been observed at numerous Southeast US monitoring sites (Budisulistiorini et al., 2013; 2015; Xu et al., 2015; Hu et al., 2015). Xu et al. (2015) concluded that IEPOX SOA may form by nucleophilic addition of sulfate (sulfate channels in Eq. (2)) leading to organosulfates. However, we find in our model that the H^+-catalyzed channel ($k_{H+}[H^+]$ term in Eq. (2)) contributes 90% of IEPOX SOA formation throughout the Southeast US boundary layer, and that sulfate channels play only a minor role. The correlation of IEPOX SOA and sulfate in the model is because increasing sulfate drives an increase in aqueous aerosol volume and acidity. Although dominance of the H^+-catalyzed channel is sensitive to uncertainties in the rate constants (Section 2), measurements from the PALMS laser mass spectrometer during SEAC^{4}RS (Liao et al., 2015) show a mean IEPOX organosulfate concentration of 0.13 μg sm^{-3}, amounting to at most 9% of total IEPOX SOA. The organosulfate should be a marker of the sulfate channels because its hydrolysis is negligibly slow (Hu et al., 2011).

Correlation between IEPOX SOA and sulfate is also apparent in the spatial distribution of IEPOX SOA, as observed by the SEAC^{4}RS aircraft below 2 km and simulated by GEOS-Chem along the aircraft flight tracks (Fig. 6). The correlation between simulated and observed IEPOX SOA in Fig. 6 is R = 0.70. Average (mean) IEPOX SOA is 1.4 ± 1.4 μg sm^{-3} in the observations and 1.3 ± 1.2 μg sm^{-3} in the model. The correlation between IEPOX SOA and sulfate is 0.66 in

the observations and 0.77 in the model. IEPOX SOA concentrations are highest in the industrial Midwest and Kentucky, and in Louisiana-Mississippi, coincident with the highest sulfate concentrations sampled on the flights. We also see in Fig. 6 frequent observations of very low IEPOX SOA (less than 0.4 μg sm^{-3}) that are well captured by the model. These are associated with very low sulfate (less than 1 μg sm^{-3}).

The mean IEPOX SOA concentration simulated by the model for the SEAC^{4}RS period (background contours in Fig. 6) is far more uniform than IEPOX SOA simulated along the flight tracks. This shows the importance of day-to-day variations in sulfate in driving IEPOX SOA variability. IEPOX SOA contributed on average 24% of total OA in the SEAC^{4}RS observations, and 28% in GEOS-Chem sampled along the flight tracks and as a regional mean. With IEPOX SOA accounting for 58% of isoprene SOA in the model (Fig. 2), this amounts to a 41-48% contribution of isoprene to total OA, consistent with the previous estimate of 40% by Kim et al. (2015).

5. Effect of Anthropogenic Emission Reductions

The EPA projects that US anthropogenic emissions of NO_x and SO_2 will decrease respectively by 34% and 48% from 2013 to 2025 (EPA, 2014). We conducted a GEOS-Chem sensitivity simulation to examine the effect of these changes on isoprene SOA, assuming no other changes and further assuming that the emission decreases are uniform across the US.

Figure 7 shows the individual and combined effects of NO_x and SO_2 emission reductions on the branching pathways for isoprene oxidation, sulfate mass concentration, aerosol pH, and isoprene SOA in the Southeast US boundary layer in summer. Reducing NO_x emission by 34% decreases the mean NO concentration by only 23%, in part because decreasing OH increases the

436 NO_x lifetime and in part because decreasing ozone increases the NO/NO_2 ratio. There is no
437 change in HO_2. We find a 10% decrease in the high-NO_x pathway and a 6% increase in the low-
438 NO_x pathway involving $ISOPO_2 + HO_2$. Aerosol sulfate decreases by 2% and there is no change
439 in $[H^+]$. The net effect is a 7% increase in isoprene SOA, as the major individual components
440 IEPOX SOA and glyoxal SOA increase by 17% and decrease by 8%, respectively.
441 A 48% decrease in SO_2 emissions drives a 36% reduction in sulfate mass concentration,
442 leading to a decline in aerosol volume (31%) that reduces uptake of all isoprene SOA precursors.
443 The decrease in aerosol $[H^+]$ (26%) further reduces IEPOX uptake. Decline in aerosol volume
444 and $[H^+]$ have a comparable effect on IEPOX SOA, as the change in each due to SO_2 emission
445 reductions is similar (~30%) and uptake of IEPOX SOA is proportional to the product of the two
446 (Section 4). IEPOX SOA and glyoxal SOA decrease by 45% and 26%, respectively, and total
447 isoprene SOA decreases by 35%. Pye et al. (2013) included uptake of IEPOX to aqueous
448 aerosols in a regional chemical transport model and similarly found that SO_2 emissions are more
449 effective than NO_x emissions at reducing IEPOX SOA in the Southeast US. Remarkably, we find
450 that reducing SO_2 emissions decreases sulfate and isoprene SOA with similar effectiveness (Fig.
451 7). With sulfate contributing ~30% of present-day $PM_{2.5}$ in the Southeast US and isoprene SOA
452 contributing ~25% (Kim et al., 2015), this represents a factor of 2 co-benefit on $PM_{2.5}$ from
453 reducing SO_2 emissions.
454
455 **6. Conclusions**
456 Standard mechanisms for formation of isoprene secondary organic aerosol (SOA) in
457 chemical transport models assume reversible partitioning of isoprene oxidation products to pre-
458 existing dry OA. This may be appropriate for dry conditions in experimental chambers but not

for typical atmospheric conditions where the aerosol is mostly aqueous. Here we developed an aqueous-phase reactive uptake mechanism coupled to a detailed gas-phase isoprene chemistry mechanism to describe the reactive uptake of water-soluble isoprene oxidation products to aqueous aerosol. We applied this mechanism in the GEOS-Chem chemical transport model to simulate surface (SOAS) and aircraft (SEAC^{4}RS) observations over the Southeast US in summer 2013.

Our mechanism includes different channels for isoprene SOA formation by the high-NO_x pathway, when the isoprene peroxy radicals ($ISOPO_2$) react with NO, and in the low-NO_x pathway where they react mostly with HO_2. The main SOA precursors are found to be isoprene epoxide (IEPOX) in the low-NO_x pathway and glyoxal in the high- and low-NO_x pathways. Both of these precursors have dominant gas-phase photochemical sinks, and so their uptake by aqueous aerosol is nearly proportional to the reactive uptake coefficient γ and to the aqueous aerosol mass concentration. The γ for IEPOX is mostly determined by the rate of H^+-catalyzed ring opening in the aqueous phase.

Application of our mechanism to the Southeast US indicates a mean isoprene SOA yield of 3.3% on a mass basis. By contrast, a conventional mechanism based on reversible uptake of semivolatile isoprene oxidation products yields only 1.1%. Simulation of the observed relationship of OA with formaldehyde (HCHO) provides support for our higher yield. We find that the low-NO_x pathway is 5 times more efficient than the high-NO_x pathway for isoprene SOA production. Under Southeast US conditions, IEPOX and glyoxal account respectively for 58% and 28% of isoprene SOA.

Our model simulates well the observations and variability of IEPOX SOA at the surface and from aircraft. The observations show a strong correlation with sulfate that we reproduce in

the model. We find this is due to the effect of sulfate on aerosol pH and volume concentration, increasing IEPOX uptake by the H^+-catalyzed ring-opening mechanism. Low concentrations of sulfate are associated with very low IEPOX SOA, both in the observations and the model, and we attribute this to the compounding effects of low sulfate on aerosol [H^+] and on aerosol volume.

The US EPA has projected that US NO_x and SO_2 emissions will decrease by 34 and 48% respectively from 2013 to 2025. We find in our model that the NO_x reduction will increase isoprene SOA by 7%, reflecting greater importance of the low-NO_x pathway. The SO_2 reduction will decrease isoprene SOA by 35%, due to decreases in both aerosol [H^+] and volume concentration. The combined effect of these two changes is to decrease isoprene SOA by 32%, corresponding to a decrease in the isoprene SOA mass yield from 3.3% to 2.3%. Decreasing SO_2 emissions by 48% has similar relative effects on sulfate (36%) and isoprene SOA (35%). Considering that sulfate presently accounts for about 30% of $PM_{2.5}$ in the Southeast US in summer, while isoprene SOA contributes 25%, we conclude that decreasing isoprene SOA represents a factor of 2 co-benefit when reducing SO_2 emissions.

Acknowledgements

We are grateful to the entire NASA SEAC^{4}RS team for their help in the field, in particular Paul Wennberg, John Crounse, Jason St. Clair, and Alex Teng for their CIT-CIMS measurements. Thanks also to Jesse Kroll for assisting in the interpretation of chamber study results. This work was funded by the NASA Tropospheric Chemistry Program, the NASA Air Quality Applied Sciences Team, and a South African National Research Foundation Fellowship and Schlumberger Faculty for the Future Fellowship to EAM. WH, JEK, PCJ, DAD, and JLJ

were supported by NASA NNX12AC03G/NNX15AT96G and NSF AGS-1243354. JEK was supported by EPA STAR (FP-91770901-0) and CIRES Fellowships. JAF acknowledges support from a University of Wollongong Vice Chancellor's Postdoctoral Fellowship. HCHO observations were acquired with support from NASA ROSES SEAC^{4}RS grant NNH10ZDA001N. Although this document has been reviewed by U.S. EPA and approved for publication, it does not necessarily reflect U.S. EPA's policies or views.

References

Anttila, T., Kiendler-Scharr, A., Tillmann, R., and Mentel, T. F.: On the reactive uptake of gaseous compounds by organic-coated aqueous aerosols: Theoretical analysis and application to the heterogeneous hydrolysis of N_2O_5, J. Phys. Chem. A, 110, 10435-10443, doi:10.1021/jp062403c, 2006.

Attwood, A. R., Washenfelder, R. A., Brock, C. A., Hu, W., Baumann, K., Campuzano-Jost, P., Day, D. A., Edgerton, E. S., Murphy, D. M., Palm, B. B., McComiskey, A., Wagner, N. L., de Sá, S. S., Ortega, A., Martin, S. T., Jimenez, J. L., and Brown, S. S.: Trends in sulfate and organic aerosol mass in the Southeast U.S.: Impact on aerosol optical depth and radiative forcing, Geophys. Res. Lett., 41, 7701-7709, doi:10.1002/2014gl061669, 2014.

Bateman, A. P., Bertram, A. K., and Martin, S. T.: Hygroscopic influence on the semisolid-to-liquid transition of secondary organic materials, J. Phys. Chem. A., 119, 4386-4395, doi:10.1021/jp508521c, 2014.

Bates, K. H., Crounse, J. D., St Clair, J. M., Bennett, N. B., Nguyen, T. B., Seinfeld, J. H., Stoltz, B. M., and Wennberg, P. O.: Gas phase production and loss of isoprene epoxydiols, J. Phys. Chem. A, 118, 1237-1246, doi:10.1021/jp4107958, 2014.

Brégonzio-Rozier, L., Giorio, C., Siekmann, F., Pangui, E., Morales, S. B., Temime-Roussel, B., Gratien, A., Michoud, V., Cazaunau, M., DeWitt, H. L., Tapparo, A., Monod, A., and Doussin, J.-F.: Secondary organic aerosol formation from isoprene photooxidation during cloud condensation–evaporation cycles, Atmos. Chem. Phys. Discuss., 15, 20561-20596, doi:10.5194/acpd-15-20561-2015, 2015.

Brown, S. S., De Gouw, J. A., Warneke, C., Ryerson, T. B., Dubé, W. P., Atlas, E., Weber, R. J., Peltier, R. E., Neuman, J. A., Roberts, J. M., Swanson, A., Flocke, F., McKeen, S. A., Brioude, J., Sommariva, R., Trainer, M., Fehsenfeld, F. C., and Ravishankara, A. R.: Nocturnal isoprene oxidation over the Northeast United States in summer and its impact on reactive nitrogen partitioning and secondary organic aerosol, Atmos. Chem. Phys., 9, 3027-3042, doi:10.5194/acp-9-3027-2009, 2009.

Budisulistiorini, S. H., Canagaratna, M. R., Croteau, P. L., Marth, W. J., Baumann, K., Edgerton, E. S., Shaw, S. L., Knipping, E. M., Worsnop, D. R., Jayne, J. T., Gold, A., and Surratt, J. D.: Real-time continuous characterization of secondary organic aerosol derived from isoprene epoxydiols in downtown Atlanta, Georgia, using the Aerodyne aerosol chemical speciation monitor, Environ. Sci. Technol., 47, 5686-5694, doi:10.1021/es400023n, 2013.

Budisulistiorini, S. H., Li, X., Bairai, S. T., Renfro, J., Liu, Y., Liu, Y. J., McKinney, K. A., Martin, S. T., McNeill, V. F., Pye, H. O. T., Nenes. A., Neff, M. E., Stone, E. A., Mueller, S., Knote, C., Shaw, S. L., Zhang, Z., Gold, A., and Surratt, J. D.: Examining the effects of anthropogenic emissions on isoprene-derived secondary organic aerosol formation during the 2013 Southern Oxidant and Aerosol Study (SOAS) at the Look Rock, Tennessee ground site, Atmos. Chem. Phys., 15, 8871-8888, doi:10.5194/acp-15-8871-2015, 2015.

Buxton, G. V., Malone, T. N., and Salmon, G. A.: Oxidation of glyoxal initiated by $^{\bullet}OH$ in oxygenated aqueous solution, J Chem. Soc. Faraday T., 93, 2889-2891, doi 10.1039/A701468f, 1997.

554 Canagaratna, M. R., Jayne, J. T., Jimenez, J. L., Allan, J. D., Alfarra, M. R, Zhang, Q., Onasch,
555 T. B., Drewnick, F., Coe, H., Middlebrook, A., Delia, A., Williams, L. R., Trimborn, A.
556 M., Northway, M. J., DeCarlo, P. F., Kolb, C. E., Davidovits, P., Worsnop, D. R.:
557 Chemical and microphysical characterization of ambient aerosols with the Aerodyne
558 Aerosol Mass Spectrometer. Mass Spectrometry Reviews, 26, 185-222, doi:
559 10.1002/mas.20115, 2007.

560 Carlton, A. G., Turpin, B. J., Altieri, K. E., Seitzinger, S. P., Mathur, R., Roselle, S. J., and
561 Weber, R. J.: CMAQ model performance enhanced when in-cloud secondary organic
562 aerosol is included: Comparisons of organic carbon predictions with measurements,
563 Environ. Sci. Technol., 42, 8789–8802, doi:1021/es801192n, 2008.

564 Carlton, A. G., Wiedinmyer, C., and Kroll, J. H.: A review of secondary organic aerosol (SOA)
565 formation from isoprene, Atmos. Chem. Phys., 9, 4987-5005, doi:10.5194/acp-9-4987-
566 2009, 2009.

567 Carlton, A. G., and Turpin, B. J.: Particle partitioning potential of organic compounds is highest
568 in the Eastern US and driven by anthropogenic water, Atmos. Chem. Phys., 13, 10203-
569 10214, doi:10.5194/acp-13-10203-2013, 2013.

570 Cazorla, M., Wolfe, G. M., Bailey, S. A., Swanson, A. K., Arkinson, H. L., and Hanisco, T. F.: A
571 new airborne laser-induced fluorescence instrument for in situ detection of formaldehyde
572 throughout the troposphere and lower stratosphere, Atmos. Meas. Tech., 8, 541-552,
573 doi:10.5194/amt-8-541-2015, 2015.

574 Chan, A. W. H., Chan, M. N., Surratt, J. D., Chhabra, P. S., Loza, C. L., Crounse, J. D., Yee, L.
575 D., Flagan, R. C., Wennberg, P. O., and Seinfeld, J. H.: Role of aldehyde chemistry and
576 NO_x concentrations in secondary organic aerosol formation, Atmos. Chem. Phys., 10,
577 7169-7188, doi:10.5194/acp-10-7169-2010, 2010.

578 Cole-Filipiak, N. C., O'Connor, A. E., and Elrod, M. J.: Kinetics of the hydrolysis of
579 atmospherically relevant isoprene-derived hydroxy epoxides, Environ. Sci. Technol., 44,
580 6718-6723, doi:10.1021/es1019228, 2010.

581 Darer, A. I., Cole-Filipiak, N. C., O'Connor, A. E., and Elrod, M. J.: Formation and stability of
582 atmospherically relevant isoprene-derived organosulfates and organonitrates, Environ. Sci.
583 Technol., 45, 1895-1902, doi:10.1021/es103797z, 2011.

584 DeCarlo, P. F., Kimmel, J. R. Trimborn, A., Northway, M. J., Jayne, J. T., Aiken, A. C., Gonin,
585 M., Fuhrer, K., Horvath, T., Docherty, K. S., Worsnop, D. R., and Jimenez, J. L.: Field-
586 deployable, High-Resolution, Time-of-Flight Aerosol Mass Spectrometer, Anal. Chem., 78,
587 8281-8289, doi: 10.1021/ac061249n, 2006.

588 Dommen, J., Metzger, A., Duplissy, J., Kalberer, M., Alfarra, M. R., Gascho, A., Weingartner,
589 E., Prévôt, A. S. H., Verheggen, B., and Baltensperger, U.: Laboratory observation of
590 oligomers in the aerosol from isoprene/NO_x photooxidation, Geophys. Res. Lett., 33,
591 L13805, doi:10.1029/2006gl026523, 2006.

592 Donahue, N. M., Robinson, A. L., Stanier, C. O., and Pandis, S. N.: Coupled partitioning,
593 dilution, and chemical aging of semivolatile organics, Environ. Sci. Technol., 40, 2635-
594 2643, doi:10.1021/es052297c, 2006.

595 Drury, E., Jacob, D. J., Spurr, R. J. D., Wang, J., Shinozuka, Y., Anderson, B. E., Clarke, A. D.,
596 Dibb, J., McNaughton, C., and Weber, R.: Synthesis of satellite (MODIS), aircraft
597 (ICARTT), and surface (IMPROVE, EPA-AQS, AERONET) aerosol observations over
598 eastern North America to improve MODIS aerosol retrievals and constrain surface aerosol
599 concentrations and sources, J. Geophys. Res., 115, D14204, doi:10.1029/2009jd012629,
600 2010.

601 EPA: U. S. Environmental Protection Agency, Technical Support Document (TSD): Preparation
602 of Emissions Inventories for the Version 6.1, 2011 Emissions Modeling Platform, available
603 at: http://www.epa.gov/ttn/chief/emch/2011v6/2011v6.1_2018_2025_base_EmisMod_TSD
604 _nov2014_v6.pdf (Accessed on July 15, 2015), 2014.

605 Eddingsaas, N. C., VanderVelde, D. G., and Wennberg, P. O.: Kinetics and products of the acid-
606 catalyzed ring-opening of atmospherically relevant butyl epoxy alcohols, J. Phys. Chem. A,
607 114, 8106-8113, doi:10.1021/jp103907c, 2010.

608 Edney, E. O., Kleindienst, T. E., Jaoui, M., Lewandowski, M., Offenberg, J. H., Wang, W., and
609 Claeys, M.: Formation of 2-methyl tetrols and 2-methylglyceric acid in secondary organic
610 aerosol from laboratory irradiated isoprene/NO_x/SO_2/air mixtures and their detection in
611 ambient $PM_{2.5}$ samples collected in the eastern United States, Atmos. Environ., 39, 5281-
612 5289, doi:10.1016/j.atmosenv.2005.05.031, 2005.

613 Ervens, B., Gligorovski, S., and Herrmann, H.: Temperature-dependent rate constants for
614 hydroxyl radical reactions with organic compounds in aqueous solutions, Phys. Chem.
615 Chem. Phys., 5, 1811-1824, doi:10.1039/b300072a, 2003.

616 Ervens, B., Turpin, B. J., and Weber, R. J.: Secondary organic aerosol formation in cloud
617 droplets and aqueous particles (aqSOA): A review of laboratory, field and model studies,
618 Atmos. Chem. Phys., 11, 11069-11102, doi:10.5194/acp-11-11069-2011, 2011.

619 Fisher, J. A., Jacob, D., Travis, K. R., Kim, P. S., Marais, E. A., Miller, C. C., Yu, K., Zhu, L.,
620 Yantosca, R. M., Sulprizio, M. P., Mao, J., Wennberg, P. O., Crounse, J. D., Teng, A. P.,
621 Nguyen, T. B., Cohen, R. C., Romer, P., Nault, B. A., Jimenez, J. L., Campuzano-Jost, P.,
622 Shepson, P. B., Xiong, F., Blake, D. R., Goldstein, A. H., Hanisco, T. F., Ryerson, T. B.,
623 Wisthaler, A., and Mikoviny, T.: Organic nitrate chemistry and its implications for nitrogen
624 budgets in and isoprene- and monoterpene-rich atmosphere: constraints from aircraft
625 (SEAC^{4}RS) and ground-based (SOAS) observations in the Southeast US, in preparation,
626 2016.

627 Fountoukis, C., and Nenes, A.: ISORROPIA II: A computationally efficient thermodynamic
628 equilibrium model for K^+-Ca^{2+}-Mg^{2+}-NH_4^+-Na^+-SO_4^{2-}-NO_3^--Cl^--H_2O aerosols, Atmos.
629 Chem. Phys., 7, 4639-4659, doi:10.5194/acp-7-4639-2007, 2007.

630 Fu, T.-M., Jacob, D. J., Wittrock, F., Burrows, J. P., Vrekoussis, M., and Henze, D. K.: Global
631 budgets of atmospheric glyoxal and methylglyoxal, and implications for formation of
632 secondary organic aerosols, J. Geophys. Res., 113, D15303, doi:10.1029/2007jd009505,
633 2008.

634 Fu, T.-M., Jacob, D. J., and Heald, C. L.: Aqueous-phase reactive uptake of dicarbonyls as a
635 source of organic aerosol over eastern North America, Atmos. Environ., 43, 1814-1822,
636 doi:10.1016/j.atmosenv.2008.12.029, 2009.

637 Gaston, C. J., Riedel, T. P., Zhang, Z., Gold, A., Surratt, J. D., and Thornton, J. A.: Reactive
638 uptake of an isoprene-derived epoxydiol to submicron aerosol particles, Environ. Sci.
639 Technol., 48, 11178-11186, doi:10.1021/es5034266, 2014.

640 González Abad, G. G., Liu, X., Chance, K., Wang, H., Kurosu, T. P., and Suleiman, R.: Updated
641 Smithsonian Astrophysical Observatory Ozone Monitoring Instrument (SAO OMI)
642 formaldehyde retrieval, Atmos. Meas. Tech., 8, 19-32, doi:10.5194/amt-8-19-2015, 2015.

643 Guenther, A., Karl, T., Harley, P., Wiedinmyer, C., Palmer, P. I., and Geron, C.: Estimates of
644 global terrestrial isoprene emissions using MEGAN (Model of Emissions of Gases and
645 Aerosols from Nature), Atmos. Chem. Phys., 6, 3181-3210, doi:10.5194/acp-6-3181-2006,
646 2006.

647 Guenther, A. B., Jiang, X., Heald, C. L., Sakulyanontvittaya, T., Duhl, T., Emmons, L. K., and
648 Wang, X.: The Model of Emissions of Gases and Aerosols from Nature version 2.1
649 (MEGAN2.1): An extended and updated framework for modeling biogenic emissions,
650 Geosci. Model Dev., 5, 1471-1492, doi:10.5194/gmd-5-1471-2012, 2012.

651 Guo, H., Xu, L., Bougiatioti, A., Cerully, K. M., Capps, S. L., Hite Jr., J. R., Carlton, A. G., Lee,
652 S.-H., Bergin, M. H., Ng, N. L., Nenes, A., and Weber, R. J.: Fine-particle water and pH in
653 the southeastern United States, Atmos. Chem. Phys., 15, 5211-5228, doi:10.5194/acp-15-
654 5211-2015, 2015.

655 Hallquist, M., Wenger, J. C., Baltensperger, U., Rudich, Y., Simpson, D., Claeys, M., Dommen,
656 J., Donahue, N. M., George, C., Goldstein, A. H., Hamilton, J. F., Herrmann, H.,
657 Hoffmann, T., Iinuma, Y., Jang, M., Jenkin, M. E., Jimenez, J. L., Kiendler-Scharr, A.,
658 Maenhaut, W., McFiggans, G., Mentel, Th. F., Monod, A., Prévôt, A. S. H., Seinfeld, J. H.,
659 Surratt, J. D., Szmigielski, R., and Wildt, J.: The formation, properties and impact of
660 secondary organic aerosol: Current and emerging issues, Atmos. Chem. Phys., 9, 5155-
661 5236, doi:10.5194/acp-9-5155-2009, 2009.

662 Hess, M., Koepke, P., and Schult, I.: Optical properties of aerosols and clouds: The software
663 package OPAC, B. Am. Meteorol. Soc., 79, 831–844, 1998.

664 Hodzic, A., and Jimenez, J. L.: Modeling anthropogenically controlled secondary organic
665 aerosols in a megacity: A simplified framework for global and climate models, Geosci.
666 Model. Dev., 4, 901-917, doi:10.5194/gmd-4-901-2011, 2011.

667 Hu, K. S., Darer, A. I., and Elrod, M. J.: Thermodynamics and kinetics of the hydrolysis of
668 atmospherically relevant organonitrates and organosulfates, Atmos. Chem. Phys., 11, 8307-
669 8320, doi:10.5194/acp-11-8307-2011, 2011.

670 Hu, W. W., Campuzano-Jost, P., Palm, B. B., Day, D. A., Ortega, A. M., Hayes, P. L.,
671 Krechmer, J. E., Chen, Q., Kuwata, M., Liu, Y. J., de Sá, S. S., Martin, S. T., Hu, M.,
672 Budisulistiorini, S. H., Riva, M., Surratt, J. D., St. Clair, J. M., Isaacman-Van Wertz, G.,
673 Yee, L. D., Goldstein, A. H., Carbone, S., Artaxo, P., de Gouw, J. A., Koss, A., Wisthaler,
674 A., Mikoviny, T., Karl, T., Kaser, L., Jud, W., Hansel, A. Docherty, K. S., Robinson, N. H.,
675 Coe, H., Allan, J. D., Canagaratna, M. R., Paulot, F., and Jimenez, J. L.: Characterization
676 of a real-time tracer for isoprene epoxydiols-derived secondary organic aerosol (IEPOX-
677 SOA) from aerosol mass spectrometer measurements, Atmos. Chem. Phys., 15, 11807–
678 11833, doi:10.5194/acp-15-11807-2015, 2015.

679 Jacob, D. J.: Heterogeneous chemistry and tropospheric ozone, Atmos. Environ., 34, 2131-2159,
680 doi:10.1016/s1352-2310(99)00462-8, 2000.

681 Jacobs, M. I., Darer, A. I., and Elrod, M. J.: Rate constants and products of the OH reaction with
682 isoprene-derived epoxides, Environ. Sci. Technol., 47, 12868-12876,
683 doi:10.1021/es403340g, 2013.

684 Jacobs, M. I., Burke, W. J., and Elrod, M. J.: Kinetics of the reactions of isoprene-derived
685 hydroxynitrates: Gas phase epoxide formation and solution phase hydrolysis, Atmos.
686 Chem. Phys., 14, 8933-8946, doi:10.5194/acp-14-8933-2014, 2014.

687 Kim, P. S., Jacob, D. J., Fisher, J. A., Travis, K., Yu, K., Zhu, L., Yantosca, R. M., Sulprizio, M.
688 P., Jimenez, J. L., Campuzano-Jost, P., Froyd, K. D., Liao, J., Hair, J. W., Fenn, M. A.,
689 Butler, C. F., Wagner, N. L., Gordon, T. D., Welti, A., Wennberg, P. O., Crounse, J. D., St.
690 Clair, J. M., Teng, A. P., Millet, D. B., Schwarz, J. P., Markovic M. Z., and Perring, A. E.:
691 Sources, seasonality, and trends of southeast US aerosol: an integrated analysis of surface,
692 aircraft, and satellite observations with the GEOS-Chem chemical transport model, Atmos.
693 Chem. Phys, 15, 10411-10433, doi:10.5194/acpd-15-10411-2015, 2015.

694 King, S. M., Rosenoern, T., Shilling, J. E., Chen, Q., Wang, Z., Biskos, G., McKinney, K. A.,
695 Pöschl, U., and Martin, S. T.: Cloud droplet activation of mixed organic-sulfate particles
696 produced by the photooxidation of isoprene, Atmos. Chem. Phys., 10, 3953-3964,
697 doi:10.5194/acp-10-3953-2010, 2010.

698 Kleindienst, T. E., Edney, E. O., Lewandowski, M., Offenberg, J. H., and Jaoui, M.: Secondary
699 organic carbon and aerosol yields from the irradiations of isoprene and α-pinene in the
700 presence of NO_x and SO_2, Environ. Sci. Technol., 40, 3807-3812, doi:10.1021/es052446r,
701 2006.

702 Kleindienst, T. E., Lewandowski, M., Offenberg, J. H., Jaoui, M., and Edney, E. O.: Ozone-
703 isoprene reaction: Re-examination of the formation of secondary organic aerosol, Geophys.
704 Res. Lett., 34, L01805, doi:10.1029/2006gl027485, 2007.

705 Kleindienst, T. E., Lewandowski, M., Offenberg, J. H., Jaoui, M., and Edney, E. O.: The
706 formation of secondary organic aerosol from the isoprene + OH reaction in the absence of
707 NO_x, Atmos. Chem. Phys., 9, 6541-6558, doi:10.5194/acp-9-6541-2009, 2009.

708 Knote, C., Hodzic, A., Jimenez, J. L., Volkamer, R., Orlando, J. J., Baidar, S., Brioude, J., Fast,
709 J., Gentner, D. R., Goldstein, A. H., Hayes, P. L., Knighton, W. B., Oetjen, H., Setyan, A.,
710 Stark, H., Thalman, R., Tyndall, G., Washenfelder, R., Waxman, E., and Zhang, Q.:
711 Simulation of semi-explicit mechanisms of SOA formation from glyoxal in aerosol in a 3-
712 D model, Atmos. Chem. Phys., 14, 6213-6239, doi:10.5194/acp-14-6213-2014, 2014.

713 Koepke, P., Hess, M., Schult, I., and Shettle, E. P.: Global aerosol data set, report, Max-Planck
714 Inst. für Meteorol., Hamburg, Germany, 1997.

715 Krechmer, J. E., Coggon, M. M., Massoli, P., Nguyen, T. B., Crounse, J. D., Hu, W., Day, D. A.,
716 Tyndall, G. S., Henze, D. K., Rivera-Rios, J. C., Nowak, J. B., Kimmel, J. R., Mauldin, III,
717 R. L., Stark, H., Jayne, J. T., Sipilä, M., Junninen, H., St. Clair, J. M., Zhang, X., Feiner, P.
718 A., Zhang, L., Miller, D. O., Brune, W. H., Keutsch, F. N., Wennberg, P. O., Seinfeld, J.
719 H., Worsnop, D. R., Jimenez, J. L., and Canagaratna, M. R.: Formation of low volatility
720 organic compounds and secondary organic aerosol from isoprene hydroxyhydroperoxide

low-NO oxidation, Environ. Sci. Technol., 49, 10330-10339, doi:10.1021/acs.est.5b02031, 2015.

Kroll, J. H., Ng, N. L., Murphy, S. M., Flagan, R. C., and Seinfeld, J. H.: Secondary organic aerosol formation from isoprene photooxidation under high-NO_x conditions, Geophys. Res. Lett., 32, L18808, doi:10.1029/2005gl023637, 2005.

Kroll, J. H., Ng, N. L., Murphy, S. M., Flagan, R. C., and Seinfeld, J. H.: Secondary organic aerosol formation from isoprene photooxidation, Environ. Sci. Technol., 40, 1869-1877, doi:10.1021/es0524301, 2006.

Lee, L., Teng, A. P., Wennberg, P. O., Crounse, J. D., and Cohen, R. C.: On rates and mechanisms of OH and O_3 reactions with isoprene-derived hydroxy nitrates, J. Phys. Chem. A, 118, 1622-1637, doi:10.1021/jp4107603, 2014.

Lewandowski, M., Jaoui, M., Offenberg, J. H., Krug, J. D., and Kleindienst, T. E.: Atmospheric oxidation of isoprene and 1,3-butadiene: Influence of aerosol acidity and relative humidity on secondary organic aerosol, Atmos. Chem. Phys., 15, 3773-3783, doi:10.5194/acp-15-3773-2015, 2015.

Liao, J., Froyd, K. D., Murphy, D. M., Keutsch, F. N., Yu, G., Wennberg, P. O., St Clair, J. M., Crounse, J. D., Wisthaler, A., Mikoviny, T., Jimenez, J. L., Campuzano-Jost, P., Day, D. A., Hu, W., Ryerson, T. B., Pollack, I. B., Peischl, J., Anderson, B. E., Ziemba, L. D., Blake, D. R., Meinardi, S., and Diskin, G.: Airborne measurements of organosulfates over the continental U.S., J. Geophys. Res., 120, 2990-3005, doi:10.1002/2014jd022378, 2015.

Liggio, J., Li, S.-M., and McLaren, R.: Reactive uptake of glyoxal by particulate matter, J. Geophys. Res., 110, D10304, doi:10.1029/2004jd005113, 2005.

Lin, Y.-H., Zhang, H., Pye, H. O. T., Zhang, Z. F., Marth, W. J., Park, S., Arashiro, M., Cui, T., Budisulistiorini, S. H., Sexton, K. G., Vizuete, W., Xie, Y., Luecken, D. J., Piletic, I. R., Edney, E. O., Bartolotti, L. J., Gold, A., and Surratt, J. D.: Epoxide as a precursor to secondary organic aerosol formation from isoprene photooxidation in the presence of nitrogen oxides, P. Natl. Acad. Sci. USA, 110, 6718-6723, doi:10.1073/pnas.1221150110, 2013.

Liu, Y. J., Herdlinger-Blatt, I., McKinney, K. A., and Martin, S. T.: Production of methyl vinyl ketone and methacrolein via the hydroperoxyl pathway of isoprene oxidation, Atmos. Chem. Phys., 13, 5715-5730, doi:10.5194/acp-13-5715-2013, 2013.

Lin, G., S. Sillman, J. E. Penner, and A. Ito, Global modeling of SOA: the use of different mechanisms for aqueous-phase formation, Atmos. Chem. Phys., 14, 5451-5475, doi:10.5194/acp-14-5451-2014, 2014.

Liu, J., L. W. Horowitz, S. Fan, A. G. Carlton, and H. Levy II, Global in-cloud production of secondary organic aerosols: implementation of a detailed chemical mechanism in the GFDL atmospheric model AM3, J. Geosphys. Res., D117, D15303, doi:10.1029/2012JD017838, 2012.

Mao, J., Paulot, F., Jacob, D. J., Cohen, R. C., Crounse, J. D., Wennberg, P. O., Keller, C. A., Hudman, R. C., Barkley, M. P., and Horowitz, L. W.: Ozone and organic nitrates over the eastern United States: Sensitivity to isoprene chemistry, J. Geophys. Res., 118, 11256-11268, doi:10.1002/jgrd.50817, 2013.

763 Martin, R. V., Jacob, D. J., Yantosca, R. M., Chin, M., and Ginoux, P.: Global and regional
764 decreases in tropospheric oxidants from photochemical effects of aerosols, J. Geophys.
765 Res., 108, 4097, doi:10.1029/2002jd002622, 2003.

766 McNeill, V. F., Woo, J. L., Kim, D. D., Schwier, A. N., Wannell, N. J., Sumner, A. J., and
767 Barakat, J. M.: Aqueous-phase secondary organic aerosol and organosulfate formation in
768 atmospheric aerosols: A modeling study, Environ. Sci. Technol., 46, 8075-8081,
769 doi:10.1021/es3002986, 2012.

770 McNeill, V. F., Sareen, N., and Schwier, A. N.: Surface-active organics in atmospheric aerosols,
771 Top. Curr. Chem., 339, 201-259, doi:10.1007/128_2012_404, 2014.

772 Millet, D. B., Jacob, D. J., Turquety, S., Hudman, R. C., Wu, S., Fried, A., Walega, J., Heikes, B.
773 G., Blake, D. R., Singh, H. B., Anderson, B. E., and Clarke, A. D.: Formaldehyde
774 distribution over North America: Implications for satellite retrievals of formaldehyde
775 columns and isoprene emission, J. Geophys. Res., 111, D24S02,
776 doi:10.1029/2005jd006853, 2006.

777 Myriokefalitakis, S., Tsigaridas, K., Mihalopoulos, N., Sciare, J., Nenes, A., Kawamura, K.,
778 Segers, A., and Kanakidou, M.: In-cloud oxalate formation in the global troposphere: a 3-D
779 modeling study, Atmos. Chem. Phys., 11, 5761-5782, doi:10.5194/acp-11-5761-2011,
780 2011.

781 Ng, N. L., Kwan, A. J., Surratt, J. D., Chan, A. W. H., Chhabra, P. S., Sorooshian, A., Pye, H. O.
782 T., Crounse, J. D., Wennberg, P. O., Flagan, R. C., and Seinfeld, J. H.: Secondary organic
783 aerosol (SOA) formation from reaction of isoprene with nitrate radicals (NO_3), Atmos.
784 Chem. Phys., 8, 4117-4140, doi:10.5194/acp-8-4117-2008, 2008.

785 Nguyen, T. B., Coggon, M. M., Bates, K. H., Zhang, X., Schwantes, R. H., Schilling, K. A.,
786 Loza, C. L., Flagan, R. C., Wennberg, P. O., and Seinfeld, J. H.: Organic aerosol formation
787 from the reactive uptake of isoprene epoxydiols (IEPOX) onto non-acidified inorganic
788 seeds, Atmos. Chem. Phys., 14, 3497-3510, doi:10.5194/acp-14-3497-2014, 2014.

789 Nguyen, T. B., Crounse, J. D., Teng, A. P., St. Clair, J. M., Paulot, F., Wolfe, G. M., and
790 Wennberg, P. O.: Rapid deposition of oxidized biogenic compounds to a temperate forest,
791 P. Natl. Acad. Sci. USA, 112, E392-E401, doi:10.1073/pnas.1418702112, 2015a.

792 Nguyen, T. B., Bates, K. H., Crounse, J. D., Schwantes, R. H., Zhang, X., Kjaergaard, H. G.,
793 Surratt, J. D., Lin, P., Laskin, A., Seinfeld, J. H., and Wennberg, P. O.: Mechanism of the
794 hydroxyl radical oxidation of methacryloyl peroxynitrate (MPAN) and its pathway toward
795 secondary organic aerosol formation in the atmosphere, Phys Chem Chem Phys, 17, 17914-
796 17926, doi:10.1039/c5cp02001h, 2015b.

797 Nozière, B., Dziedzic, P., and Córdova, A.: Products and kinetics of the liquid-phase reaction of
798 glyoxal catalyzed by ammonium ions (NH_4^+), J. Phys. Chem. A, 113, 231-237,
799 doi:10.1021/jp8078293, 2009.

800 Odum, J. R., Hoffmann, T., Bowman, F., Collins, D., Flagan, R. C., and Seinfeld, J. H.:
801 Gas/particle partitioning and secondary organic aerosol yields, Environ. Sci. Technol., 30,
802 2580-2585, doi:10.1021/es950943+, 1996.

Palmer, P. I., Jacob, D. J., Fiore, A. M., Martin, R. V., Chance, K., and Kurosu, T. P.: Mapping isoprene emissions over North America using formaldehyde column observations from space, J. Geophys. Res., 108, 4180, doi:10.1029/2002jd002153, 2003.

Palmer, P. I., Abbot, D. S., Fu, T.-M., Jacob, D. J., Chance, K., Kurosu, T. P., Guenther, A., Wiedinmyer, C., Stanton, J. C., Pilling, M. J., Pressley, S. N., Lamb, B., and Sumner, A. L.: Quantifying the seasonal and interannual variability of North American isoprene emissions using satellite observations of the formaldehyde column, J. Geophys. Res., 111, D12315, doi:10.1029/2005jd006689, 2006.

Paulot, F., Crounse, J. D., Kjaergaard, H. G., Kroll, J. H., Seinfeld, J. H., and Wennberg, P. O.: Isoprene photooxidation: New insights into the production of acids and organic nitrates, Atmos. Chem. Phys., 9, 1479-1501, doi:10.5194/acp-9-1479-2009, 2009a.

Paulot, F., Crounse, J. D., Kjaergaard, H. G., Kürten, A., St Clair, J. M., Seinfeld, J. H., and Wennberg, P. O.: Unexpected epoxide formation in the gas-phase photooxidation of isoprene, Science, 325, 730-733, doi:10.1126/science.1172910, 2009b.

Peeters, J., Nguyen, T. L., and Vereecken, L.: HO_x radical regeneration in the oxidation of isoprene, Phys. Chem. Chem. Phys., 11, 5935-5939, doi:10.1039/b908511d, 2009.

Peeters, J., and Müller, J.-F.: HO_x radical regeneration in isoprene oxidation via peroxy radical isomerisations. II: Experimental evidence and global impact, Phys. Chem. Chem. Phys., 12, 14227-14235, doi:10.1039/c0cp00811g, 2010.

Piletic, I. R., Edney, E. O., and Bartolotti, L. J.: A computational study of acid catalyzed aerosol reactions of atmospherically relevant epoxides, Phys. Chem. Chem. Phys., 15, 18065-18076, doi:10.1039/c3cp52851k, 2013.

Pye, H. O. T., Chan, A. W. H., Barkley, M. P., and Seinfeld, J. H.: Global modeling of organic aerosol: The importance of reactive nitrogen (NO_x and NO_3), Atmos. Chem. Phys., 10, 11261-11276, doi:10.5194/acp-10-11261-2010, 2010.

Pye, H. O. T., Pinder, R. W., Piletic, I. R., Xie, Y., Capps, S. L., Lin, Y.-H., Surratt, J. D., Zhang, Z., Gold, A., Luecken, D. J., Hutzell, W. T., Jaoui, M., Offenberg, J. H., Kleindienst, T. E., Lewandowski, M., and Edney, E. O.: Epoxide pathways improve model predictions of isoprene markers and reveal key role of acidity in aerosol formation, Environ. Sci. Technol., 47, 11056-11064, doi:10.1021/es402106h, 2013.

Riedel, T. P., Lin, Y.-H., Budisulistiorini, S. H., Gaston, C. J., Thornton, J. A., Zhang, Z. F., Vizuete, W., Gold, A., and Surratt, J. D.: Heterogeneous reactions of isoprene-derived epoxides: Reaction probabilities and molar secondary organic aerosol yield estimates, Environ. Sci. Technol. Lett., 2, 38-42, doi:10.1021/ez500406f, 2015.

Rollins, A. W., Kiendler-Scharr, A., Fry, J. L., Brauers, T., Brown, S. S., Dorn, H.-P., Dubé, W. P., Fuchs, H., Mensah, A., Mentel, T. F., Rohrer, F., Tillmann, R., Wegener, R., Wooldridge, P. J., and Cohen, R. C.: Isoprene oxidation by nitrate radical: Alkyl nitrate and secondary organic aerosol yields, Atmos. Chem. Phys., 9, 6685-6703, doi:10.5194/acp-9-6685-2009, 2009.

SEAC^{4}RS Archive, doi:10.5067/Aircraft/SEAC4RS/Aerosol-TraceGas-Cloud.

Sato, K., Nakao, S., Clark, C. H., Qi, L., and Cocker III, D. R.: Secondary organic aerosol formation from the photooxidation of isoprene, 1,3-butadiene, and 2,3-dimethyl-1,3-butadiene under high NO_x conditions, Atmos. Chem. Phys., 11, 7301-7317, doi:10.5194/acp-11-7301-2011, 2011.

Saxena, P., and Hildemann, L. M.: Water-soluble organics in atmospheric particles: A critical review of the literature and application of thermodynamics to identify candidate compounds, J. Atmos. Chem., 24, 57-109, doi:10.1007/bf00053823, 1996.

Schwartz, S.E.: Mass-transport considerations pertinent to aqueous-phase reactions of gases in liquid-water clouds. In: Jaechske, W. (Ed.), Chemistry of Multiphase Atmospheric Systems, Springer, Heidelberg, pp. 415-471, 1986.

Scott, C. E., Rap, A., Spracklen, D. V., Forster, P. M., Carslaw, K. S., Mann, G. W., Pringle, K. J., Kivekäs, N., Kulmala, M., Lihavainen, H., and Tunved, P.: The direct and indirect radiative effects of biogenic secondary organic aerosol, Atmos. Chem. Phys., 14, 447-470, doi:10.5194/acp-14-447-2014, 2014.

Song, M., Liu, P. F., Hanna, S. J., Li, Y. J., Martin, S. T., and Bertram, A. K.: Relative humidity-dependent viscosities of isoprene-derived secondary organic material and atmospheric implications for isoprene-dominant forests, Atmos. Chem. Phys., 15, 5145-5159, doi:10.5194/acp-15-5145-2015, 2015.

Stavrakou, T., Peeters, J., and Müller, J.-F.: Improved global modelling of HO_x recycling in isoprene oxidation: Evaluation against the GABRIEL and INTEX-A aircraft campaign measurements, Atmos. Chem. Phys., 10, 9863-9878, doi:10.5194/acp-10-9863-2010, 2010.

St. Clair, J. M., Rivera-Rios, J. C., Crounse, J. D., Knap, H. C., Bates, K. H., Teng, A. P., Jørgensen, S., Kjaergaard, H. G., Keutsch, F. N., Wennberg, P. O.: Kinetics and products of the reaction of the first-generation isoprene hydroperoxide (ISOPOOH) with OH, J. Phys. Chem. A, doi:10.1021/acs.jpca.5b06532, 2016.

Sumner, A. J., Woo, J. L., and McNeill, V. F.: Model Analysis of secondary organic aerosol formation by glyoxal in laboratory studies: The case for photoenhanced chemistry, Environ. Sci. Technol., 48, 11919-11925, doi:10.1021/es502020j, 2014.

Surratt, J. D., Murphy, S. M., Kroll, J. H., Ng, N. L., Hildebrandt, L., Sorooshian, A., Szmigielski, R., Vermeylen, R., Maenhaut, W., Claeys, M., Flagan, R. C., and Seinfeld, J. H.: Chemical composition of secondary organic aerosol formed from the photooxidation of isoprene, J. Phys. Chem. A, 110, 9665-9690, doi:10.1021/jp061734m, 2006.

Surratt, J. D., Lewandowski, M., Offenberg, J. H., Jaoui, M., Kleindienst, T. E., Edney, E. O., and Seinfeld, J. H.: Effect of acidity on secondary organic aerosol formation from isoprene, Environ. Sci. Technol., 41, 5363-5369, doi:10.1021/es0704176, 2007a.

Surratt, J. D., Kroll, J. H., Kleindienst, T. E., Edney, E. O., Claeys, M., Sorooshian, A., Ng, N. L., Offenberg, J. H., Lewandowski, M., Jaoui, M., Flagan, R. C., and Seinfeld, J. H.: Evidence for organosulfates in secondary organic aerosol, Environ. Sci. Technol., 41, 517-527, doi:10.1021/es062081q, 2007b.

Surratt, J. D., Chan, A. W. H., Eddingsaas, N. C., Chan, M., Loza, C. L., Kwan, A. J., Hersey, S. P., Flagan, R. C., Wennberg, P. O., and Seinfeld, J. H.: Reactive intermediates revealed in

884 secondary organic aerosol formation from isoprene, P. Natl. Acad. Sci. USA, 107, 6640-
885 6645, doi:10.1073/pnas.0911114107, 2010.

886 Tan, Y., Perri, M. J., Seitzinger, S. P., and Turpin, B. J.: Effects of precursor concentration and
887 acidic sulfate in aqueous glyoxal-OH radical oxidation and implications for secondary
888 organic aerosol, Environ. Sci. Technol., 43, 8105-8112, doi:10.1021/es901742f, 2009.

889 Tan, Y., Carlton, A. G., Seitzinger, S. P., and Turpin, B. J.: SOA from methylglyoxal in clouds
890 and wet aerosols: Measurement and prediction of key products, Atmos. Environ., 44, 5218-
891 5226, doi:10.1016/j.atmosenv.2010.08.045, 2010.

892 Toon, O. B. and the SEAC^{4}RS science team: Planning, implementation, and scientific goals of
893 the Studies of Emissions and Atmospheric Composition, Clouds, and Climate Coupling by
894 Regional Surveys (SEAC^{4}RS) field mission, submitted to J. Geosphys. Res., 2016.

895 Travis, K. R., Jacob, D. J., Fisher, J. A., Kim, P. S., Marais, E. A., Zhu, L., Miller, C. C.,
896 Wennberg, P. O., Crounse, J., Hanisco, T. A., Ryerson, T., Yu, K., Wolfe, G. M.,
897 Thompson, A., Mao, J., Paulot, F., Yantosca, R. M., Sulprizio, M., and Neuman, A.: NO_x
898 emissions, isoprene oxidation pathways, and implications for surface ozone in the
899 Southeast United States, in preparation, 2016.

900 Virtanen, A., Joutsensaari, J., Koop, T., Kannosto, J., Yli-Pirilä, P., Leskinen, J., Mäkelä, J. M.,
901 Holopainen, J. K., Pöschl, U., Kulmala, M., Worsnop, D. R., and Laaksonen, A.: An
902 amorphous solid state of biogenic secondary organic aerosol particles, Nature, 467, 824-
903 827, doi:10.1038/nature09455, 2010.

904 Volkamer, R., Martini, F. S., Molina, L. T., Salcedo, D., Jimenez, J. L., and Molina, M. J.: A
905 missing sink for gas-phase glyoxal in Mexico City: Formation of secondary organic
906 aerosol, Geophys. Res. Lett., 34, L19807, doi:10.1029/2007gl030752, 2007.

907 Volkamer, R., Ziemann, P. J., and Molina, M. J.: Secondary organic aerosol formation from
908 acetylene (C_2H_2): Seed effect on SOA yields due to organic photochemistry in the aerosol
909 aqueous phase, Atmos. Chem. Phys., 9, 1907-1928, doi:10.5194/acp-9-1907-2009, 2009.

910 Wagner, N. L., Brock, C. A., Angevine, W. M., Beyersdorf, A., Campuzano-Jost, P., Day, D., de
911 Gouw, J. A., Diskin, G. S., Gordon, T. D., Graus, M. G., Holloway, J. S., Huey, G.,
912 Jimenez, J. L., Lack, D. A., Liao, J., Liu, X., Markovic, M. Z., Middlebrook, A. M.,
913 Mikoviny, T., Peischl, J., Perring, A. E., Richardson, M. S., Ryerson, T. B., Schwarz, J. P.,
914 Warneke, C., Welti, A., Wisthaler, A., Ziemba, L. D., and Murphy, D. M.: In situ vertical
915 profiles of aerosol extinction, mass, and composition over the southeast United States
916 during SENEX and SEAC^{4}RS: Observations of a modest aerosol enhancement aloft,
917 Atmos. Chem. Phys., 15, 7085-7102, doi:10.5194/acp-15-7085-2015, 2015.

918 Wang, J., Hoffmann, A. A., Park, R. J., Jacob, D. J., and Martin, S. T.: Global distribution of
919 solid and aqueous sulfate aerosols: Effect of the hysteresis of particle phase transitions, J.
920 Geophys. Res., 113, D11206, doi:10.1029/2007jd009367, 2008.

921 Waxman, E. M., Dzepina, K., Ervens, B., Lee-Taylor, J., Aumont, B., Jimenez, J. L., Madronich,
922 S., and Volkamer, R.: Secondary organic aerosol formation from semi- and intermediate-
923 volatility organic compounds and glyoxal: Relevance of O/C as a tracer for aqueous
924 multiphase chemistry, Geophys. Res. Lett., 40, 978-982, doi:10.1002/grl.50203, 2013.

925 Xu, L., Kollman, M. S., Song, C., Shilling, J. E., and Ng, N. L.: Effects of NO_x on the volatility
926 of secondary organic aerosol from isoprene photooxidation, Environ. Sci. Technol., 48,
927 2253-2262, doi:10.1021/es404842g, 2014.

928 Xu, L., Guo, H., Boyd, C. M., Klein, M., Bougiatioti, A., Cerully, K. M., Hite, J. R., Isaacman-
929 VanWertz, G., Kreisberg, N. M., Knote, C., Olson, K., Koss, A., Goldstein, A. H., Hering,
930 S. V., de Gouw, J., Baumann, K., Lee, S.-H., Nenes, A., Weber, R. J., and Ng, N. L.:
931 Effects of anthropogenic emissions on aerosol formation from isoprene and monoterpenes
932 in the southeastern United States, P. Natl. Acad. Sci. USA, 112, 37-42,
933 doi:10.1073/pnas.1417609112, 2015.

934 Yu, K., Jacob, D. J., Fisher, J., Kim, P. S., Marais, E. A., Miller, C. C., Travis, K., Zhu, L.,
935 Yantosca, R. M., Sulprizio, M., Cohen, R. C., Dibb, J. E., Fried, A., Mikoviny, T., Ryerson,
936 T. B., Wennberg, P. O., and Wisthaler, A.: Sensitivity to grid resolution in the ability of a
937 chemical transport model to simulate observed oxidant chemistry under high-isoprene
938 conditions, submitted to Atmos. Chem. Phys., 2016.

939 Zhang, Q., Jimenez, J. L., Canagaratna, M. R., Allan, J. D., Coe, H., Ulbrich, I., Alfarra, M. R.,
940 Takami, A., Middlebrook, A. M., Sun, Y. L., Dzepina, K., Dunlea, E., Docherty, K.,
941 DeCarlo, P. F., Salcedo, D., Onasch, T., Jayne, J. T., Miyoshi, T., Shimono, A.,
942 Hatakeyama, S., Takegawa, N., Kondo, Y., Schneider, J., Drewnick, F., Borrmann, S.,
943 Weimer, S., Demerjian, K., Williams, P., Bower, K., Bahreini, R., Cottrell, L., Griffin, R.
944 J., Rautiainen, J., Sun, J. Y., Zhang, Y. M., and Worsnop, D. R.: Ubiquity and dominance
945 of oxygenated species in organic aerosols in anthropogenically-influenced Northern
946 Hemisphere midlatitudes, Geophys. Res. Lett., 34, L13801, doi:10.1029/2007gl029979,
947 2007.

948 Zhang, H., Surratt, J. D., Lin, Y. H., Bapat, J., and Kamens, R. M.: Effect of relative humidity on
949 SOA formation from isoprene/NO photooxidation: Enhancement of 2-methylglyceric acid
950 and its corresponding oligoesters under dry conditions, Atmos. Chem. Phys., 11, 6411-
951 6424, doi:10.5194/acp-11-6411-2011, 2011.

952 Zhang, H., Parikh, H. M., Bapat, J., Lin, Y. H., Surratt, J. D., and Kamens, R. M.: Modelling of
953 secondary organic aerosol formation from isoprene photooxidation chamber studies using
954 different approaches, Environ. Chem., 10, 194-209, doi:10.1071/en13029, 2013.

955 Zhu, L., Jacob, D., Mickley, L., Kim, P. S., Fisher, J., Travis, K., Yu, K., Yantosca, R. M.,
956 Sulprizio, M., Fried, A., Hanisco, T., Wolfe, G., Abad, G. G., Chance, K., De Smedt, I.,
957 and Yang, K.: Indirect validation of new OMI, GOME-2, and OMPS formaldehyde
958 (HCHO) retrievals using $SEAC^4RS$ data, in preparation, 2016.

TABLES

Table 1. Constants for reactive uptake of isoprene SOA precursors [a]

Species [b]	H^* [M atm^{-1}]	k_{H+} [M^{-1} s^{-1}]	k_{nuc} [M^{-2} s^{-1}]	k_{HSO4-} [M^{-1} s^{-1}]	k_{aq} [s^{-1}]
IEPOX	3.3×10^{7}, [c]	3.6×10^{-2}, [d]	2.0×10^{-4}, [e]	7.3×10^{-4}, [e]	Equation (2)
$ISOPN_\beta$ [f]	3.3×10^{5}, [g]	–	–	–	1.6×10^{-5}, [h]
$ISOPN_\delta$ [f]	3.3×10^{5}, [g]	–	–	–	6.8×10^{-3}, [h]
DHDN	3.3×10^{5}, [g]	–	–	–	6.8×10^{-3}, [i]

[a] Effective Henry's law constants H^* and aqueous-phase rate constants used to calculate reactive uptake coefficients γ for isoprene SOA precursors IEPOX, $ISOPN_\beta$, $ISOPN_\delta$, and DHDN following Eqs. (1) and (2). Calculation of γ for other isoprene SOA precursors in Fig. 2 is described in the text.

[b] See Fig. 2 for definition of acronyms.

[c] Best fit to SOAS and SEAC^{4}RS IEPOX SOA and consistent with Nguyen et al. (2014).

[d] Cole-Filipiak et al. (2010).

[e] Eddingsaas et al. (2010).

[f] ISOPN species formed from the beta and delta isoprene oxidation channels (Paulot et al., 2009a) are treated separately in GEOS-Chem.

[g] By analogy with 4-nitrooxy-3-methyl-2-butanol (Rollins et al., 2009).

[h] Jacobs et al. (2014).

[i] Assumed same as for $ISOPN_\delta$ (Hu et al., 2011).

973 **Table 2.** Mean reactive uptake coefficients γ of isoprene SOA precursors [a]

Species [b]	γ	pH dependence [c]			
		pH > 3	2 < pH < 3	1 < pH < 2	0 < pH < 1
IEPOX	4.2×10^{-3}	8.6×10^{-7}	2.0×10^{-4}	1.1×10^{-3}	1.0×10^{-2}
MEPOX	1.3×10^{-4}	2.7×10^{-8}	6.4×10^{-6}	3.6×10^{-5}	3.2×10^{-4}
$ISOPN_{\beta}$	1.3×10^{-7}	–			
$ISOPN_{\delta}$	5.2×10^{-5}	–			
DHDN	6.5×10^{-5}	–			
GLYX	2.9×10^{-3} [d]	–			
MGLY	4.0×10^{-7}	–			
C_5-LVOC	0.1	–			
NT-ISOPN	0.1	–			

974 [a] Mean values computed in GEOS-Chem for the Southeast US in summer as sampled along the boundary-
975 layer (< 2 km) SEAC^{4}RS aircraft tracks and applied to aqueous aerosol. The reactive uptake coefficient γ
976 is defined as the probability that a gas molecule colliding with an aqueous aerosol particle will be taken
977 up and react in the aqueous phase to form non-volatile products.

978 [b] See Fig. 2 for definition of acronyms.

979 [c] γ for IEPOX and MEPOX are continuous functions of pH (Eq. (2)). Values shown here are averages for
980 different pH ranges sampled along the SEAC^{4}RS flight tracks. Aqueous aerosol pH is calculated locally
981 in GEOS-Chem using the ISORROPIA thermodynamic model (Fountoukis and Nenes, 2007).

982 [d] Daytime value. Nighttime value is 5×10^{-6}.

983

FIGURES

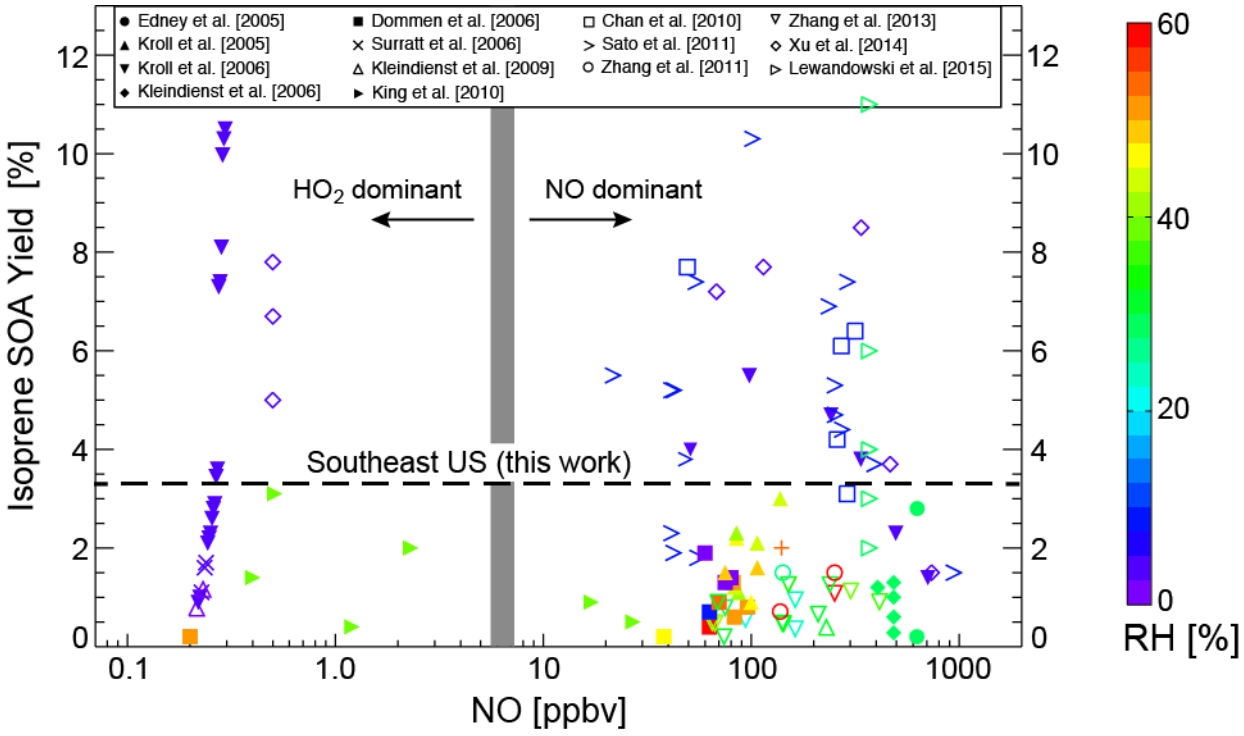

Figure 1. Yields of secondary organic aerosol (SOA) from isoprene oxidation as reported by chamber studies in the literature and plotted as a function of the initial NO concentration and relative humidity (RH). Yields are defined as the mass of SOA produced per unit mass of isoprene oxidized. For studies with no detectable NO we plot the NO concentration as half the reported instrument detection limit, and stagger points as needed for clarity. Data are colored by relative humidity (RH). The thick grey line divides the low-NO_x and high-NO_x pathways as determined by the fate of the $ISOPO_2$ radical (HO_2 dominant for the low-NO_x pathway, NO dominant for the high-NO_x pathway). The transition between the two pathways occurs at a higher NO concentration than in the atmosphere because HO_2 concentrations in the chambers are usually much higher. Also shown as dashed line is the mean atmospheric yield of 3.3% for the Southeast US determined in our study.

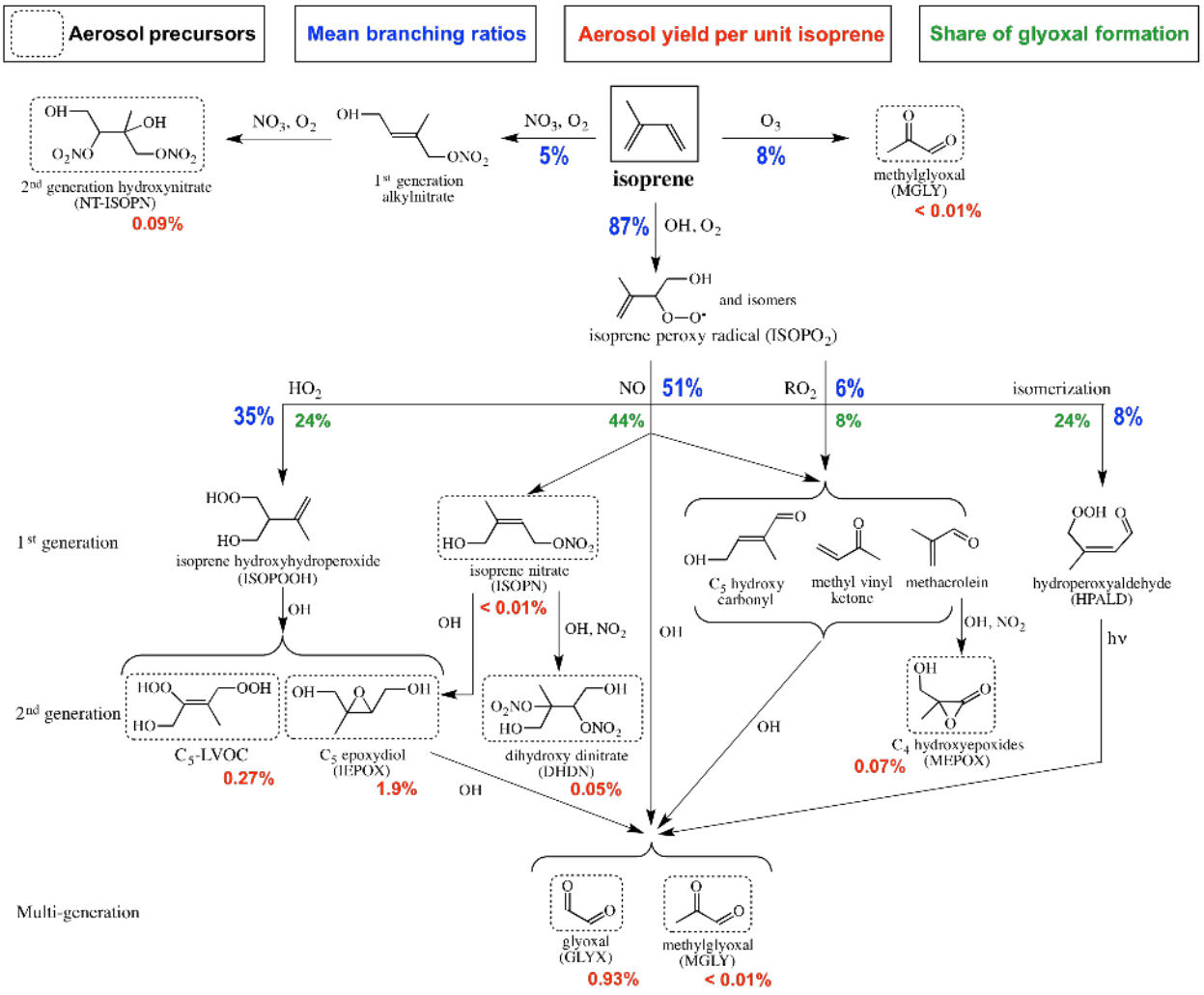

999

1000 **Figure 2.** Gas-phase isoprene oxidation cascade in GEOS-Chem leading to secondary organic
1001 aerosol (SOA) formation by irreversible aqueous-phase chemistry. Only selected species relevant
1002 to SOA formation are shown. Immediate aerosol precursors are indicated by dashed boxes.
1003 Branching ratios and SOA yields (aerosol mass produced per unit mass isoprene reacted) are
1004 mean values from our GEOS-Chem simulation for the Southeast US boundary layer in summer.
1005 The total SOA yield from isoprene oxidation is 3.3% and the values shown below the dashed
1006 boxes indicate the contributions from the different immediate precursors adding up to 3.3%.
1007 Contributions of high- and low-NO_x isoprene oxidation pathways to glyoxal are indicated.

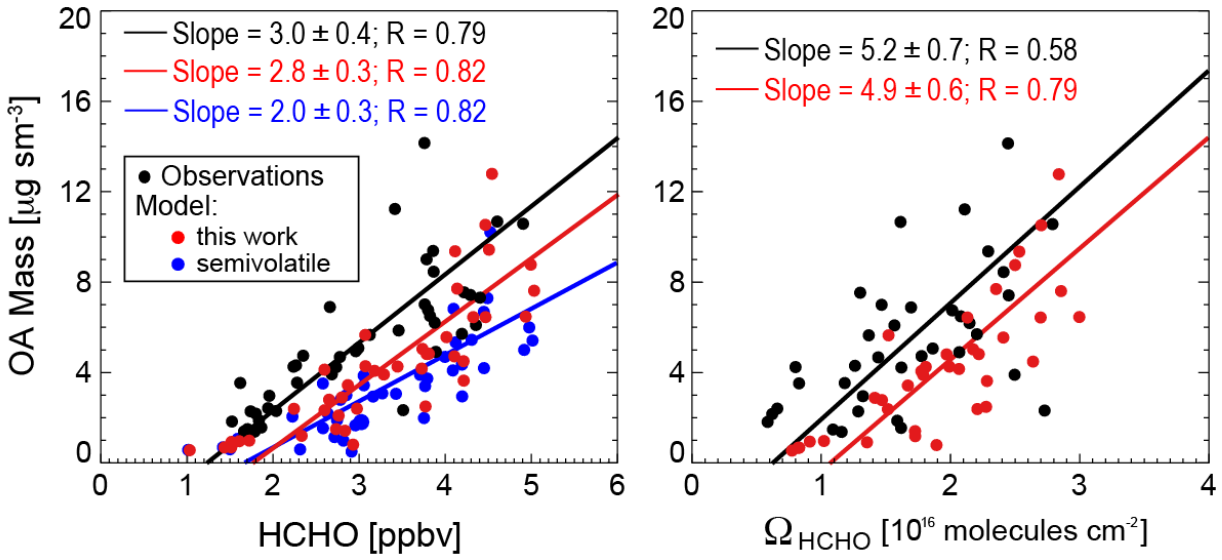

1008

1009 **Figure 3.** Relationship of organic aerosol (OA) and formaldehyde (HCHO) concentrations over
1010 the Southeast US in summer. The figure shows scatterplots of SEAC^{4}RS aircraft observations of
1011 OA concentrations in the boundary layer (< 2 km) vs. HCHO mixing ratios measured from the
1012 aircraft (left), and column HCHO (Ω_{HCHO}) retrieved from OMI satellite observations (right).
1013 Individual points are data from individual SEAC^{4}RS flight days (August 8 - September 10),
1014 averaged on the GEOS-Chem grid. OMI data are for SEAC^{4}RS flight days and coincident with
1015 the flight tracks. GEOS-Chem is sampled for the corresponding locations and times. Results
1016 from our simulation with aqueous-phase isoprene SOA chemistry are shown in red, and results
1017 from a simulation with the Pye et al. (2010) semivolatile reversible partitioning scheme are
1018 shown in blue. Aerosol concentrations are per m^3 at standard conditions of temperature and
1019 pressure (STP: 273 K; 1 atm), denoted sm^{-3}. Reduced major axis (RMA) regressions are also
1020 shown with regression parameters and Pearson's correlation coefficients given inset. 1σ standard
1021 deviations on the regression slopes are obtained with jackknife resampling.

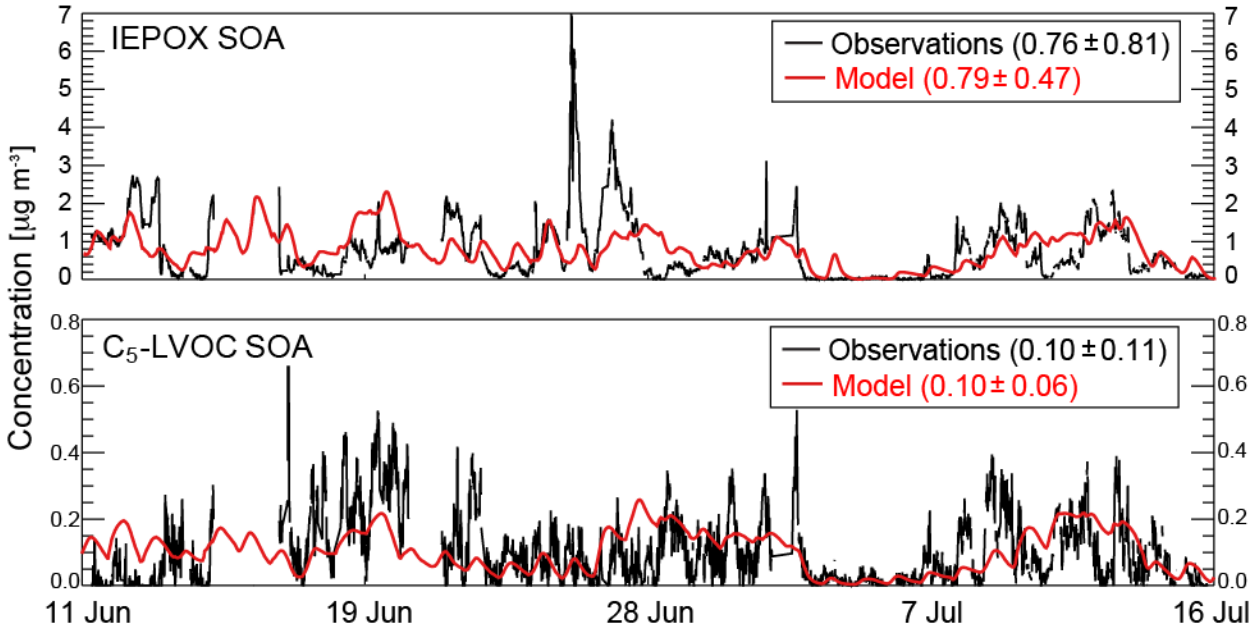

1022

1023

1024 **Figure 4.** Time series of the concentrations of isoprene SOA components at the SOAS site in
1025 Centreville, Alabama (32.94°N; 87.18°W) in June-July 2013: measured (black) and modeled
1026 (red) IEPOX SOA (top) and C_5-LVOC SOA (bottom) mass concentrations. Means and 1σ
1027 standard deviations are given for the observations and the model.

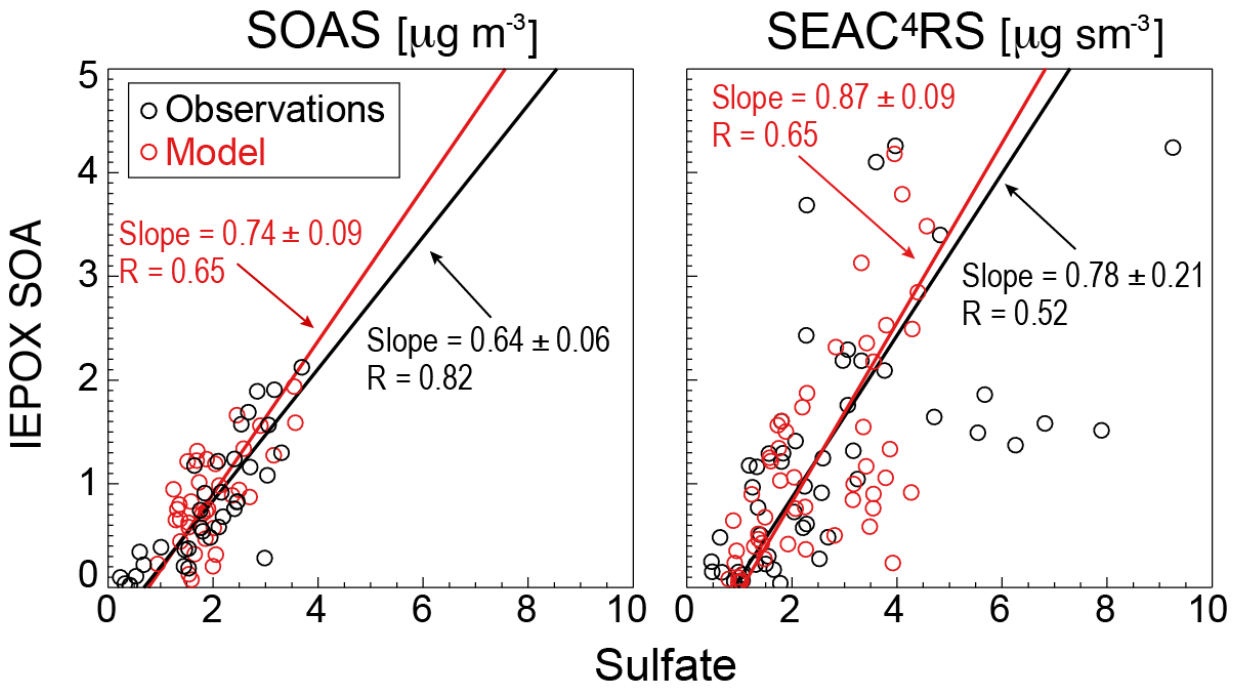

1028

1029 **Figure 5.** Relationship of IEPOX SOA and sulfate concentrations over the Southeast US in
1030 summer. Observed (black) and simulated (red) data are averages for each campaign day during
1031 SOAS (left), and boundary layer averages (< 2 km) for 2° × 2.5° GEOS-Chem grid squares on
1032 individual flight days during SEAC^{4}RS (right). RMA regression slopes and Pearson's correlation
1033 coefficients are shown. 1σ standard deviations on the regression slopes are obtained with
1034 jackknife resampling.

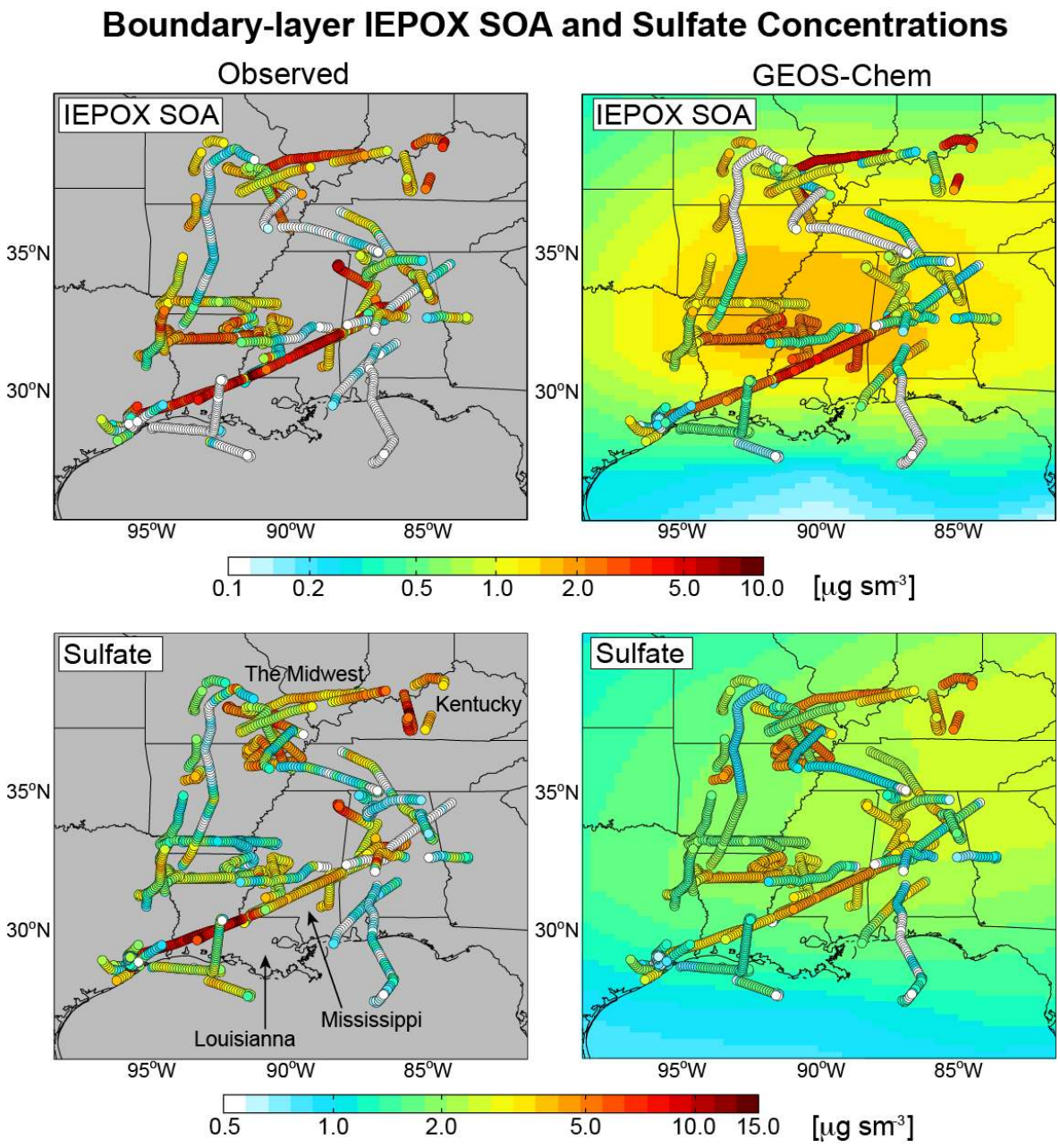

1035

1036 **Figure 6.** Spatial distributions of IEPOX SOA and sulfate concentrations in the boundary layer
1037 (<2 km) over the Southeast US during SEAC[4]RS (August-September 2013). Aircraft AMS
1038 observations of IEPOX SOA (top left) and sulfate (bottom left) are compared to model values
1039 sampled at the time and location of the aircraft observations (individual points) and averaged
1040 during the SEAC[4]RS period (background contours). Data are on a logarithmic scale.
1041

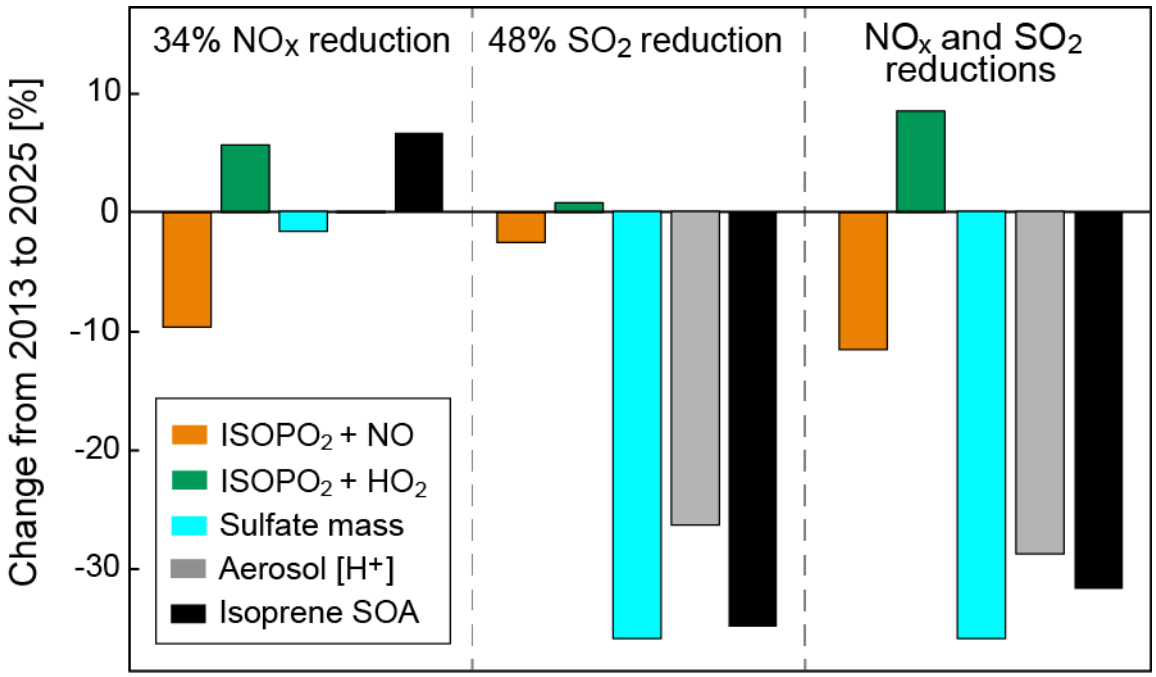

1042

1043

1044 **Figure 7.** Effect of projected 2013-2025 reductions in US anthropogenic emissions on the
1045 formation of isoprene secondary organic aerosol (SOA). Emissions of NO_x and SO_2 are projected
1046 to decrease by 34% and 48%, respectively. Panels show the resulting percentage changes in the
1047 branching of $ISOPO_2$ between the NO and HO_2 oxidation channels, sulfate mass concentration,
1048 aerosol $[H^+]$ concentration, and isoprene SOA mass concentration. Values are summer means for
1049 the Southeast US boundary layer.

1050